Atmos. Chem. Phys. Discuss., https://doi.org/10.5194/acp-2019-108
Manuscript under review for journal Atmos. Chem. Phys.
Discussion started: 4 March 2019

Atmospheric Chemistry and Physics Discussions

Nitrification of the lowermost stratosphere during the exceptionally cold Arctic winter 2015/16

Marleen Braun[1], Jens-Uwe Grooß[2], Wolfgang Woiwode[1], Sören Johansson[1], Michael Höpfner[1], Felix Friedl-Vallon[1], Hermann Oelhaf[1], Peter Preusse[2], Jörn Ungermann[2], Björn-Martin Sinnhuber[1], Helmut Ziereis[3], and Peter Braesicke[1]

[1]Institute of Meteorology and Climate Research, Karlsruhe Institute of Technology, Karlsruhe, Germany
[2]Institute of Energy- and Climate Research, Stratosphere (IEK-7), Forschungszentrum Jülich, Jülich, Germany
[3]Institute of Atmospheric Physics, German Aerospace Center, Oberpfaffenhofen, Germany

Correspondence: Marleen Braun (marleen.braun@kit.edu)

Abstract. The Arctic winter 2015/16 was characterized by exceptionally cold stratospheric temperatures, favouring the formation of polar stratospheric clouds (PSCs) from mid-December until the end of February down to low stratospheric altitudes. Observations by GLORIA (Gimballed Limb Observer for Radiance Imaging of the Atmosphere) on HALO (High Altitude and LOng range research aircraft) during the PGS (POLSTRACC/GW-LCYLCE II/SALSA) campaign from December 2015 to March 2016 allow an investigation of the influence of denitrification on the lowermost stratosphere (LMS) with a high spatial resolution. For the first time vertical cross-sections of nitric acid (HNO_3) along the flight track and tracer-tracer correlations derived from the GLORIA observations document detailed pictures of wide-spread nitrification of the Arctic LMS during the course of an entire winter. GLORIA observations show large-scale structures and local fine structures with strongly enhanced absolute HNO_3 volume mixing ratios reaching up to 11 ppbv at altitudes of 11 km in January and nitrified filaments persisting until the middle of March. Narrow streaks of enhanced HNO_3, observed in mid-January, are interpreted as regions recently nitrified by sublimating HNO_3-containing particles. Overall, a nitrification of the LMS between 5.0 ppbv and 7.0 ppbv at potential temperature levels between 350 and 380 K is estimated. This extent of nitrification has never been observed before in the Arctic lowermost stratosphere. The GLORIA observations are compared with CLaMS (Chemical Lagrangian Model of the Stratosphere) simulations. The fundamental structures observed by GLORIA are well reproduced, but differences in the fine structures are diagnosed. Further, CLaMS predominantly underestimates the spatial extent of maximum HNO_3 mixing ratios derived from the GLORIA observations as well as the enhancement at lower altitudes. Sensitivity simulations with CLaMS including (i) enhanced sedimentation rates in case of ice supersaturation (to resemble ice nucleation on NAT), (ii) a global temperature offset, (iii) modified growth rates (to resemble aspherical particles with larger surfaces) and (iv) temperature fluctuations (to resemble the impact of small-scale mountain waves) mostly improve the agreement with the GLORIA observations. The sensitivity simulations suggest that details of particle microphysics play a significant role for simulated LMS nitrification in January, while air subsidence, transport and mixing become increasingly important towards the end of the winter.

Atmos. Chem. Phys. Discuss., https://doi.org/10.5194/acp-2019-108
Manuscript under review for journal Atmos. Chem. Phys.
Discussion started: 4 March 2019

Atmospheric Chemistry and Physics Discussions

1 Introduction

The processes of denitrification and nitrification are well-known phenomena occurring in the polar winter stratosphere (Fahey et al., 1990). They involve the condensation, growth, sedimentation and sublimation of nitric acid (HNO_3)-containing polar stratospheric cloud (PSC) particles and result in an irreversible vertical redistribution of HNO_3. Denitrification is known to affect polar winter ozone loss (Fahey et al., 1990; Waibel, 1999). While denitrification at higher layers (i.e. around 16 to 22 km) attenuates fast deactivation of catalytically active chlorine species into the reservoir species chlorine nitrate ($ClONO_2$), chlorine deactivation can be fostered at lower layers enriched in HNO_3 (i.e. nitrified) by evaporating nitric acid trihydrate (NAT) particles (Fischer et al., 1997). Observational evidence for particles other than NAT involved in denitrification is sparse (e.g. Tabazadeh and Toon, 1996; Kim et al., 2006). Nitrification of the lowermost stratosphere is of particular interest since the chemical budget of reactive nitrogen (NO_y) and, thereby, its possible effects on ozone are modified in a region important for the radiative budget of the atmosphere (Riese et al., 2012).

While fundamental processes in connection with PSCs are well understood, there are still uncertainties concerning the formation of NAT particles and their characteristics that influence the processes of denitrification and nitrification. Chemistry-transport and global chemistry models including simplified microphysical properties of NAT are generally successful in simulating denitrification of the polar winter stratospheres (Carslaw, 2002; Grooß et al., 2005, 2014; Khosrawi et al., 2017; Zhu et al., 2017, and references therein). However, parametrizations resulting in agreement with observed size distributions of NAT particles, particularly extremely large NAT particles, and reproducing fine-structures of observed denitrification patterns remain an issue (e.g. Molleker et al., 2014; Woiwode et al., 2014).

Hemispheric differences in nitrification are observed due to different conditions in Antarctic and Arctic winter vortices. In the Antarctic, cold and stable vortices result in widespread PSC coverage and denitrification over wide vertical ranges. PSCs are observed less frequently in the Arctic, and the degree of denitrification varies from winter to winter (Santee et al., 1999; Pitts et al., 2018, and references therein). Increasing greenhouse gas emissions could lead to lower stratospheric temperatures (e.g. Rex et al., 2006) which likely cause stronger denitrification of the Arctic stratosphere.

Numerous studies addressed denitrification in Arctic winters, especially in cold winters, e.g. 1994/1995 (Waibel, 1999), 1999/2000 (Popp et al., 2001), 2004/2005 (Jin et al., 2006), 2009/2010 (Khosrawi et al., 2011; Woiwode et al., 2014), 2010/2011 (Sinnhuber et al., 2011) and 2015/2016 (Khosrawi et al., 2017). While most of these studies focused on the denitrification at altitudes higher than roughly 15 km, less attention was paid to the associated nitrification of lower layers. Only Dibb et al. (2006) reported nitrification at potential temperature levels above 340 K (around 12 km) at the end of January 2005. Particularly, nitrification of the Arctic lowermost stratosphere (LMS) has hardly been investigated. This is due to the fact that cold winters with strong denitrification were rare events in the Arctic stratosphere in the past and that the observational capabilities to resolve nitrification of the LMS with sufficient coverage and vertical resolution are sparse. For example, limb-sounders, like MLS (Microwave Limb Sounder; Waters et al., 2006) or MIPAS (Michelson Interferometer for Passive Atmospheric Sounding; Fischer et al., 2008) typically have vertical resolutions of around 3-5 km making it difficult to resolve fine-scale structures of NO_y redistribution.

Atmos. Chem. Phys. Discuss., https://doi.org/10.5194/acp-2019-108
Manuscript under review for journal Atmos. Chem. Phys.
Discussion started: 4 March 2019

Atmospheric Chemistry and Physics Discussions

The process of vertical HNO_3 redistribution is very sensitive to temperature. NAT particle nucleation can begin as soon as temperatures fall below NAT equilibrium temperature T_{NAT}. NAT particles are nucleated heterogeneously with low number densities on foreign nuclei such as meteoritic dust particles (Hoyle et al., 2013). Below T_{NAT}, these particle grow and sediment downward and they evaporate as temperatures rise above T_{NAT}. A simulation of this process is challenging as it depends both on the nucleation parametrisation and on the precise reproduction of the temperatures around T_{NAT}. This is especially the case during the onset of this process. At a later time, the vertical HNO_3 redistribution may be saturated as due to the lower HNO_3 mixing ratio, no additional NAT particles can be nucleated. Since both the nucleation process and the mesoscale temperature is not well known, it is especially difficult to simulate the small-scale structure of HNO_3 during the onset period.

Here, we present observations of nitrification of the LMS in the unusually cold Arctic winter 2015/2016 by the airborne limb-imaging Fourier transform infra red (FTIR) spectrometer GLORIA (Gimballed Limb Observer for Radiance Imaging of the Atmosphere, Friedl-Vallon et al. (2014); Riese et al. (2014)). In that winter, an extraordinarily cold and stable polar vortex (Matthias et al., 2016; Manney and Lawrence, 2016) promoted a long-lasting PSC phase from mid-December until the end of February with a large vertical extent (Pitts et al., 2018; Voigt et al., 2018) reaching down into the LMS.

Using the GLORIA observations, we investigate the evolution of nitrification in the LMS during the course of the winter. Additionally, we attempt to quantify the observed nitrification, which is particularly difficult because the LMS composition is influenced by air masses originating from the Arctic vortex, the extra-vortex stratosphere and the troposphere (Werner et al., 2010; Gettelman et al., 2011; Krause et al., 2018).

Furthermore, we compare the GLORIA data with simulations by the Chemical Lagrangian Model of the Stratosphere (CLaMS; Grooß et al., 2014, references therein) and test how well different parametrizations within the model reproduce the GLORIA observations.

2 Aircraft Campaign and Data

2.1 POLSTRACC/GW-LCYCLE II/SALSA

The GLORIA observations analysed in this study were obtained during the combined POLSTRACC (POLar STRAtosphere in a Changing Climate), GW-LCYCLE II (Gravity Wave Life Cycle Experiment) and SALSA (Seasonality of Air mass transport and origin in the Lowermost Stratosphere using the HALO Aircraft) campaigns (PGS). Starting from Oberpfaffenhofen, Germany or Kiruna, Sweden 18 research flights were carried out by the German research aircraft HALO (High Altitude and LOng range research aircraft) between December 2015 and March 2016. The flights probed an entire winter period in the LMS at high northern latitudes.

2.2 GLORIA

GLORIA is an airborne infrared limb imaging spectrometer (Friedl-Vallon et al., 2014). During PGS, GLORIA has been operated on board the HALO aircraft and pointed to the right hand side of the flight path. GLORIA combines a Michelson

interferometer with an imaging HgCdTe detector which records 128 vertical and 48 horizontal interferograms simultaneously. All interferograms are transformed into spectra and spectra from horizontal detector rows are averaged for noise reduction prior to the atmospheric parameter retrieval (Kleinert et al., 2014). In high spectral resolution mode, which is used in this study, the spectrometer covers the range from 780 to 1400 cm^{-1} with a spectral sampling of 0.0625 cm^{-1}. For the retrieval, the radiative transfer code KOPRA (Karlsruhe Optimized and Precise Radiation transfer Algorithm; Stiller et al., 2002) and the inversion tool KOPRAFIT (Höpfner et al., 2001) were used. Estimated uncertainties of the GLORIA retrieval results are typically 1 - 2 K for temperature and 10 - 20% for trace gases. Typical vertical resolutions of the retrieved profiles are about 400 m at flight altitude and decrease to about 1000 m around the lowest tangent points. A detailed description and validation of the dataset used in this study is given by Johansson et al. (2018).

2.3 CLaMS

The Chemical Lagrangian Model of the Stratosphere (CLaMS) (McKenna, 2002a, b) is a chemistry transport model based on trajectory calculations for an ensemble of air parcels. CLaMS includes modules simulating Lagrangian trajectories, mixing, chemical processes and Lagrangian particle sedimentation. The CLaMS simulations used here were performed with a special setup for the POLSTRACC campaign with a horizontal resolution of about 100 km and a vertical resolution of about 500-900 m in the lower stratosphere above 10 km altitude decreasing to about 2 km below 9 km altitude. Further, this configuration includes a comprehensive stratospheric chemistry as described by Grooß et al. (2014). The simulations were performed for the entire winter and were based on meteorological wind and temperature data from the ECMWF ERA interim reanalysis (Dee et al., 2011) employing a horizontal resolution of 1x1 degrees and a timestep of 6 h. To simulate processes connected to NAT particles, particle parcels are implemented (Grooß et al., 2005, 2014). Particle size and number concentration are assigned to each particle parcel so that various particle parcels in one air parcel determine the particle size distribution. NAT and ice nucleation is temperature and saturation dependent and is parametrized by the scheme by Hoyle et al. (2013) and Engel et al. (2013), respectively. Particle growth and evaporation are calculated along particle trajectories based on Carslaw (2002) assuming the characteristics of spherical particles (Tritscher et al., 2018). Comparisons with PSC observations (Tritscher et al., 2018) show that the parametrisation of nucleation and sedimentation of NAT and ice particles in CLaMS is capable to reproduce the main features of PSC observations. Also, vortex averages of the vertical redistribution of HNO_3 and H_2O have been reproduced.

3 Methods

3.1 GLORIA vertical cross sections of atmospheric parameters

The GLORIA retrieval results in vertical atmospheric parameter profiles. These vertical profiles are combined to 2-dimensional quasi-vertical cross sections along the flight paths and show mesoscale atmospheric structures (Johansson et al., 2018). Since the observations are performed in limb-mode, the distance of the tangent points (i.e where the major information about

Atmos. Chem. Phys. Discuss., https://doi.org/10.5194/acp-2019-108
Manuscript under review for journal Atmos. Chem. Phys.
Discussion started: 4 March 2019

atmospheric parameters stems from) gradually increases from the observer for the lower limb views. This is reflected by the tangent point distributions in Figs. 1a, 2a, 3a and 4a. The GLORIA data is filtered for cloud-affected observations, and data points with a vertical resolution worse than 2 km or above flight altitude are neglected for further analysis.

3.2 Simulated cross sections from CLaMS

For comparison with GLORIA, the CLaMS data were interpolated to the retrieval grid geolocations, characterized by altitude, latitude, longitude and time of the tangent points. The temporal interpolation with respect to atmospheric dynamics is performed by trajectory calculations. CLaMS output is typically saved daily at 12:00 UTC. Therefore forward trajectories are calculated for points between 00:00 UTC and 12:00 UTC until 12:00 UTC. The corresponding 12:00 UTC volume mixing ratio is then assumed as concentration of the original geolocation based on the assumption that chemical and physical changes in volume mixing ratios during the time of the trajectory calculations are negligible for the chemical species considered here. For points between 12:00 UTC and 00:00 UTC backward trajectories are calculated analogously.

3.3 Identification of sub-vortex air

The altitude range of GLORIA observations in this study typically lies within the LMS, ranging from the tropopause to the 380 K isentrope (see Werner et al., 2010, and references therein). It has to be pointed out that robust identification of vortex air in the LMS is not possible due to dynamical disturbances, transport and in-mixing of air masses from different origins. In fact, the sub-vortex region in the LMS has a more filamentary character and is affected by interaction with air masses from the extra-vortex stratospheric overworld, the extra-tropical transition layer (ExTL), and the troposphere (Gettelman et al., 2011). Two filters have been applied in order to select data points associated with the sub-vortex region.

The first filter applied is the criterion by Nash et al. (1996) at the 370 K isentrope and based on the PV field obtained from the Merra-2 reanalysis. Grid points with latitude-longitude pairs outside the polar vortex at the potential temperature (θ) level of 370 K are classified as non-vortex points. Secondly, data is filtered by scaled potential vorticity (sPV) calculated from Merra-2 reanalysis data with a threshold of $1.2 \cdot 10^{-4} s^{-1}$. sPV is calculated by dividing the potential vorticity (PV) by $\partial\theta/\partial p$ to obtain similar PV ranges for all isentropic levels that are investigated (Manney et al., 1994; Dunkerton and Delisi, 1986). Therefore this filter takes the altitude information of the grid points into account. Data points in the tracer correlations (see below) are attributed to sub-vortex air, if both criteria are met.

4 GLORIA observations and CLaMS simulations of selected flights from January to March 2016

4.1 Flight 6 on 12 January 2016

Flight 6 started on 12 January 2016 from Oberpfaffenhofen as the transfer flight to Kiruna. At the flight day, the identified vortex region (indicated by non-shaded areas in Fig. 1a) appears relatively coherent by applying the Nash criterion at θ =

Atmos. Chem. Phys. Discuss., https://doi.org/10.5194/acp-2019-108
Manuscript under review for journal Atmos. Chem. Phys.
Discussion started: 4 March 2019

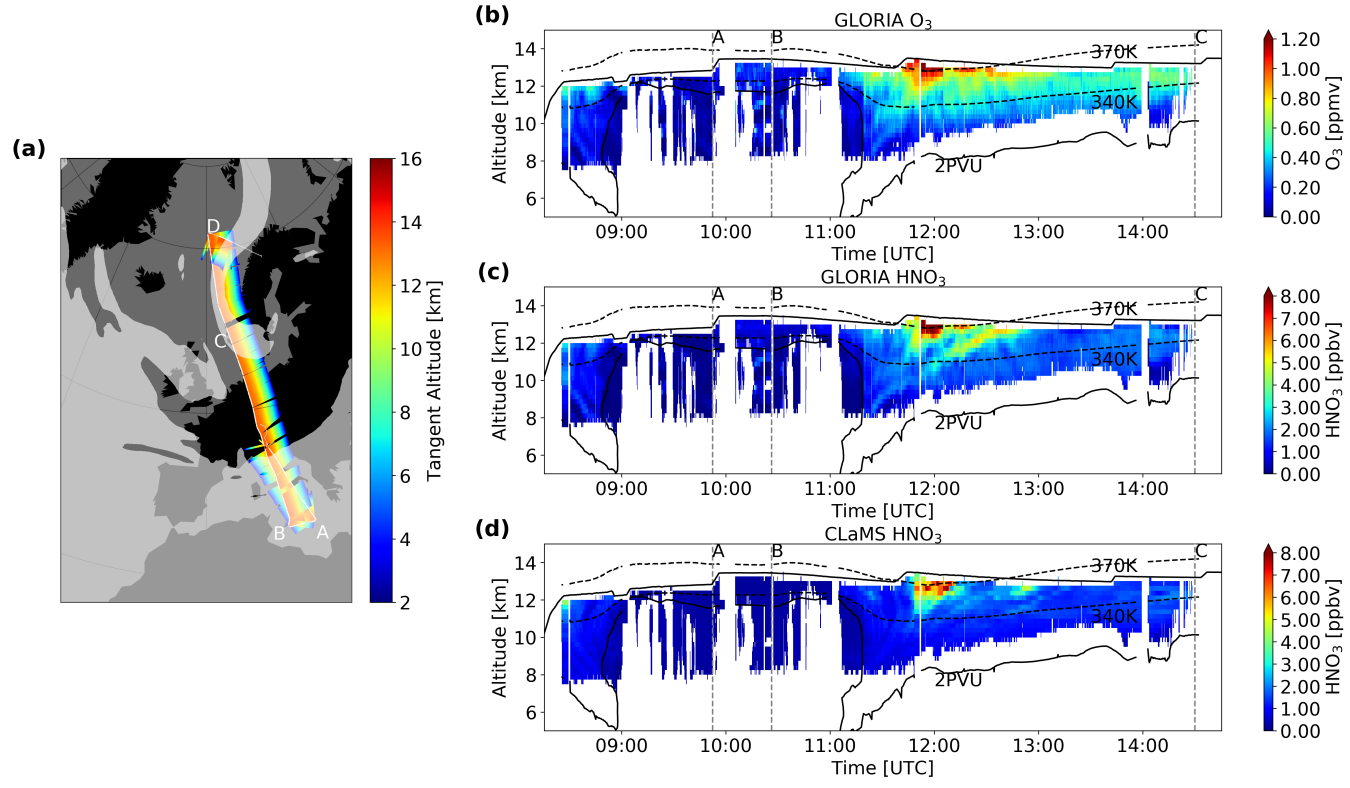

Figure 1. (a) Flight path and vortex filtering according to the Nash criterion at 370 K for flight 6 on 12 January 2016. White line: flight track with characteristic waypoints (A, B); light grey shading: areas that are not associated with the polar vortex. Cross-sections of (b) O_3 and (c) HNO_3 distribution derived from GLORIA and (d) HNO_3 distribution simulated by CLaMS for flight 6 on 12 January 2016. Flight altitude (bold black line), characteristic waypoints (A, B), 340 K and 370 K potential temperature levels (ECMWF, dashed black lines) and 2 PVU level (ECMWF, black line).

370 K. Only above the British Isles, southern Scandinavia and north-west of Norway patches of air masses do not fulfil this filter criterion. Further, PSCs were observed above flight altitude towards the end of the flight near Kiruna (Pitts et al., 2018).

Maximum ozone volume mixing ratios of 1.2 ppmv are observed between 11:40 and 12:10 UTC close to the flight altitude (Fig. 1b). Except for flight segments with a high tropopause (indicated by the 2 PVU level) from 09:00 to 11:20 UTC outside the vortex region, ozone volume mixing ratios of about 0.5 ppmv are observed around the 340 K isentrope. The HNO_3 volume mixing ratios (Fig. 1c) show a more complex pattern. The structures until 11:20 UTC show a similar pattern as ozone, corresponding with the non vortex region. Further, maximum HNO_3 volume mixing ratios well exceeding 8 ppbv are observed around 12:00 UTC close to flight altitude. While the ozone distribution after 12:00 UTC appears relatively coherent along an isentrope, values differ significantly for HNO_3. Here, maximum values spread over fewer data points. Moreover, a band-like structure of enhanced HNO_3 values appears between 12:00 and 13:00 UTC. In summary, the observed HNO_3 structures exhibit

Atmos. Chem. Phys. Discuss., https://doi.org/10.5194/acp-2019-108
Manuscript under review for journal Atmos. Chem. Phys.
Discussion started: 4 March 2019

a much larger spatial variability than those observed in the ozone distribution, indicating their formation due to redistribution processes.

The modelled HNO_3 volume mixing ratios (Fig. 1d) show a maximum of 8 ppbv between 11:50 and 12:20 UTC at altitudes between 12 and 13 km, well matching the location where the maximum is observed by GLORIA. Further, CLaMS models slightly enhanced HNO_3 volume mixing ratios at flight altitude at 12:50 UTC corresponding to the maximum of the band-like structure observed by GLORIA. Compared to the observations, CLaMS shows a similar overall structure but is not able to reproduce the band-like structure. CLaMS underestimates the maximum HNO_3 volume mixing ratios for most flight segments and doesn't model an enhancement down to the same altitudes as observed by GLORIA. We point out that enhancements at low altitudes are potentially not well reproduced due to the model's low vertical resolution of about 2 km at altitudes below 9 km.

4.2 Flight 8 on 20 January 2016

The flight on 20 January 2016 started and ended in Kiruna and took place during in the coldest phase of the winter (Manney and Lawrence, 2016). Applying the Nash criterion a relatively coherent vortex region is found, with all GLORIA tangent points located inside the vortex region at θ = 370K (Fig. 2a). The flight was carried out during particularly cold conditions, with PSCs ranging down to flight level. Since clouds complicate a robust trace gas retrieval, a number of GLORIA observations where sorted out by cloud-filtering. As a consequence, only limited GLORIA nitric acid data are available in flight sections with sufficiently transparent conditions (Fig. 2b). Further, particulate NO_y was simultaneously measured in-situ by using a chemiluminescence-detector in combination with a converter for NO_y species (Stratmann et al., 2016). Similar observations have also been made during other aircraft campaigns in the Arctic (Northway et al., 2002). NO_y-containing particles were detected as gas phase-equivalent NO_y*. In Fig. 2c, we show the measurements taken during the flight on 20 January 2016 which are not corrected for enhancement efficiency (Ziereis et al., 2004). We use the data as a proxy for condensed particulate HNO_3 present at flight altitude. The in situ data clearly confirm the presence of HNO_3-containing PSC particles at flight altitude and in the vicinity of the local HNO_3 maxima detected by GLORIA.

The vertical cross-sections of O_3 and HNO_3 volume mixing ratios along the HALO flight track derived from GLORIA are depicted in Fig. 2b, d. The ozone distribution shows increasing volume mixing ratios with altitude reaching 1.1 ppmv at 13 km. The observed O_3 volume mixing ratios vary only moderately at fixed altitude levels during the whole flight in agreement with the location of the measurements within the vortex and the homogeneity inside the vortex. The HNO_3 distribution shows enhanced HNO_3 volume mixing ratios particularly in the flight segment between the waypoints C and D, reaching up to 8 ppbv at a flight altitude of 13 km compared to 3 ppbv observed in adjacent air around waypoint D. Enhanced values are forming band-like structures and are observed down to 11 km in that flight segment. Further, small scale fine structures with enhanced HNO_3 volume mixing ratios appear between 15:30 and 17:00 UTC and reach down to 10 km. The pattern of continuous and slightly tilted vertical bands differ significantly from the ozone distribution, indicating their formation by redistribution of HNO_3. The simultaneous presence of confined local gas phase HNO_3 maxima in the GLORIA data and HNO_3-containing particles detected in situ suggests that an ongoing nitrification process was probed.

Atmos. Chem. Phys. Discuss., https://doi.org/10.5194/acp-2019-108
Manuscript under review for journal Atmos. Chem. Phys.
Discussion started: 4 March 2019

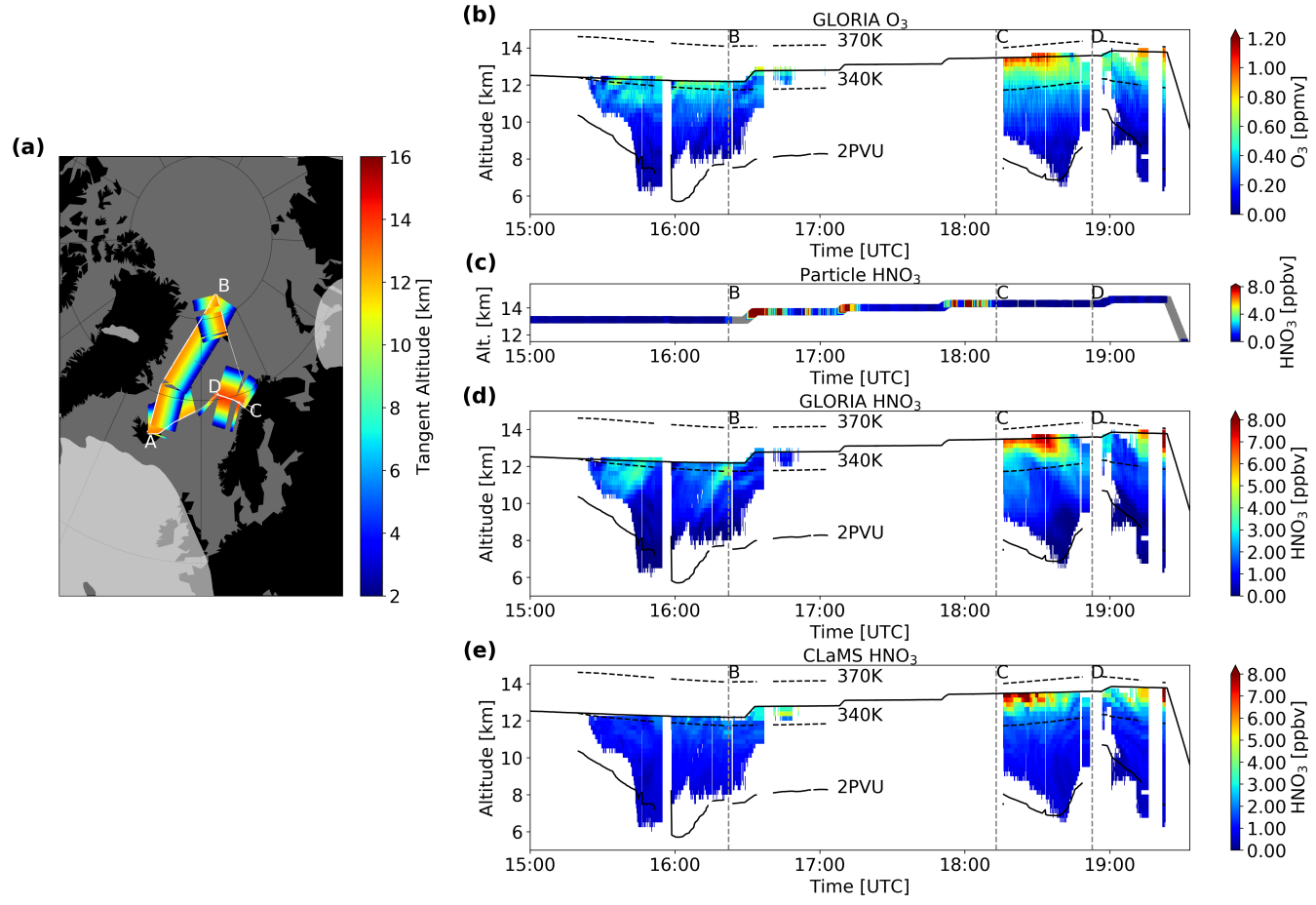

Figure 2. (a) Flight path and vortex filtering according to the Nash criterion at 370 K for flight 8 on 20 January 2016. White line: flight track with characteristic waypoints (A, B, C, D); light grey shading: areas that are not associated with the polar vortex. Cross-sections of (b) O_3 and (d) HNO_3 distribution derived from GLORIA and (e) HNO_3 distribution simulated by CLaMS for flight 8 on 20 January 2016. Flight altitude (bold black line), characteristic waypoints (B, C, D), 340 K and 370 K potential temperature levels (ECMWF, dashed black lines) and 2 PVU level (ECMWF, black line). (c) Particulate nitrate measurements at flight altitude for flight 8 on 20 January 2016 (not enhancement corrected)

The vertical cross-section of HNO_3 volume mixing ratios modelled by CLaMS is shown in Fig. 2e. HNO_3 volume mixing ratios reach maximum values of 8 ppbv at flight altitude in the flight segment between C and D. While maximum HNO_3 volume mixing ratios in this flight are well represented by CLaMS, slight differences in the location of the maximum occur. Enhanced HNO_3 volume mixing ratios reach down to only 11 km compared to 9 km for the GLORIA observations. Additionally, CLaMS shows slightly enhanced HNO_3 volume mixing ratios around 16:00 UTC but does not represent the small scale fine structures observed between 15:30 and 17:00 UTC.

Atmos. Chem. Phys. Discuss., https://doi.org/10.5194/acp-2019-108
Manuscript under review for journal Atmos. Chem. Phys.
Discussion started: 4 March 2019

Atmospheric Chemistry and Physics Discussions

4.3 Flight 12 on 31 January 2016

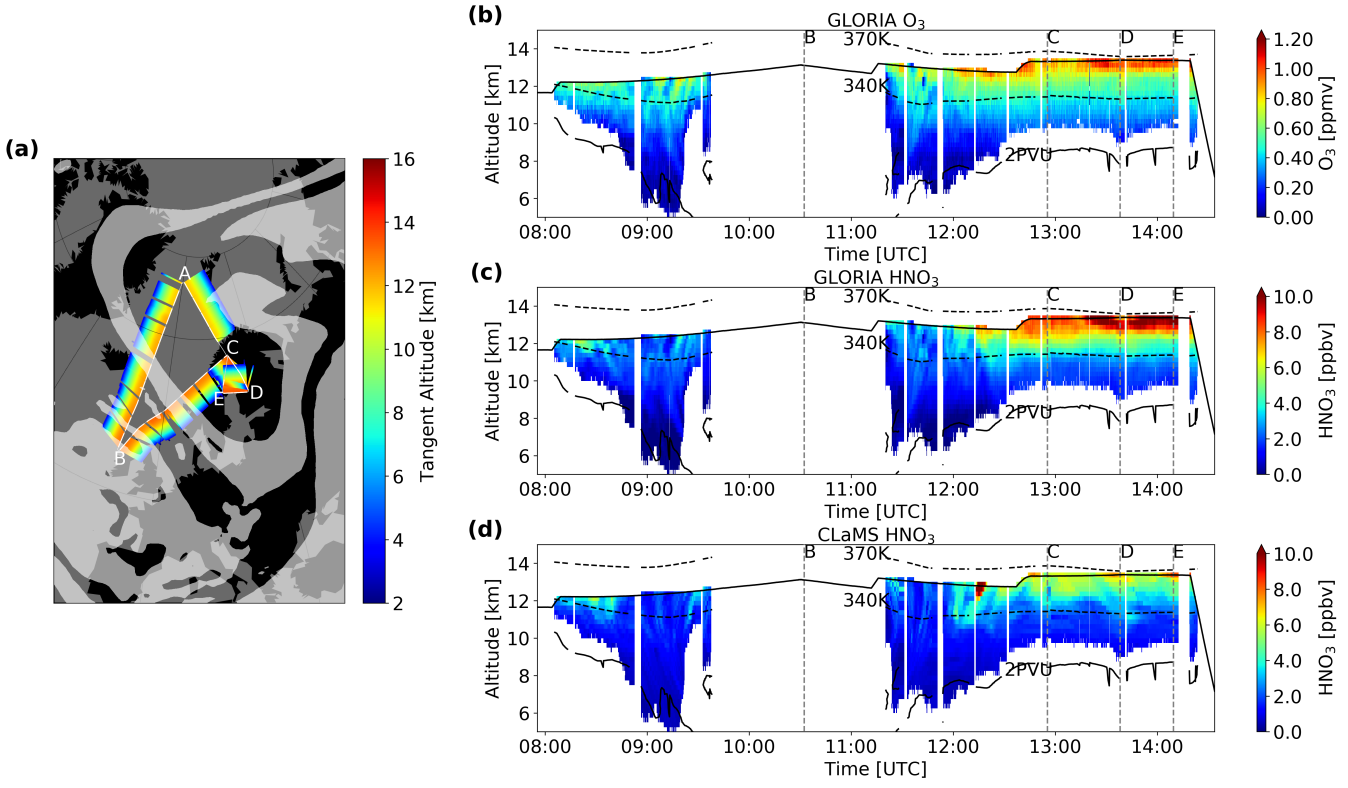

Figure 3. (a) Flight path and vortex filtering according to the Nash criterion at 370 K for flight 12 on 31 January 2016. White line: flight track with characteristic waypoints (A, B, C, D, E); light grey shading: areas that are not associated with the polar vortex. Cross-sections of (b) O_3 and (c) HNO_3 distribution derived from GLORIA and (d) HNO_3 distribution simulated by CLaMS for flight 12 on 31 January 2016. Flight altitude (bold black line), characteristic waypoints (B, C, D, E), 340 K and 370 K potential temperature levels (ECMWF, dashed black lines) and 2 PVU level (ECMWF, black line). Please note the changed colorbar for HNO_3 compared to Figs. 1,2,4.

At the end of January 2016, applying the Nash criterion at θ = 370K, a more disturbed lower vortex region is observed. As shown in Fig. 3a, a large region between Greenland, central Europe and northern Siberia fulfilled the vortex criterion. However, filaments of lower PV are found from Greenland to southern Scandinavia and around the eastern rim of Scandinavia. Flight 12 was carried out starting and ending in Kiruna on 31 January and intersected several times with filaments outside the vortex.

Measured cross-sections of O_3 and HNO_3 volume mixing ratios are depicted in Fig. 3b and 3c. Except for the flight segments between 8:40 UTC and 9:20 UTC as well as 11:30 UTC and 11:50 UTC, that are associated with vortex edge or non vortex air, ozone values increasing with height are observed. During this flight, enhanced HNO_3 volume mixing ratios of up to 6 ppbv are measured around 8:15 UTC at flight altitude. Additionally, a pattern of strongly enhanced HNO_3 volume mixing ratios appears between 12:15 and 14:30 UTC at altitudes from 11 to 14 km, reaching maximum values well above 10 ppbv between 13:30

Atmos. Chem. Phys. Discuss., https://doi.org/10.5194/acp-2019-108
Manuscript under review for journal Atmos. Chem. Phys.
Discussion started: 4 March 2019

Atmospheric Chemistry and Physics Discussions

and 14:30 UTC slightly below flight altitude. Since those structures between waypoints C and E vary significantly from those observed in the ozone concentrations they most likely originated from nitrification.

The HNO_3 distribution modelled by CLaMS is shown in Fig. 3d. Around 8:10 UTC enhanced HNO_3 volume mixing ratios of 6 ppbv are modelled. Further, enhanced HNO_3 volume mixing ratios are modelled after 12:15 UTC reaching down to altitudes of 12 km, slightly higher in altitude than for the GLORIA observations. Maximum HNO_3 volume mixing ratios are found at flight altitude showing narrow peaks up to 10 ppbv at 12:15 UTC and 8 ppbv at 12:50 UTC, at waypoint D and E. Overall, CLaMS shows a higher spatial variability and underestimates the maximum values during large parts of the flight.

4.4 Flight 21 on 18 March 2016

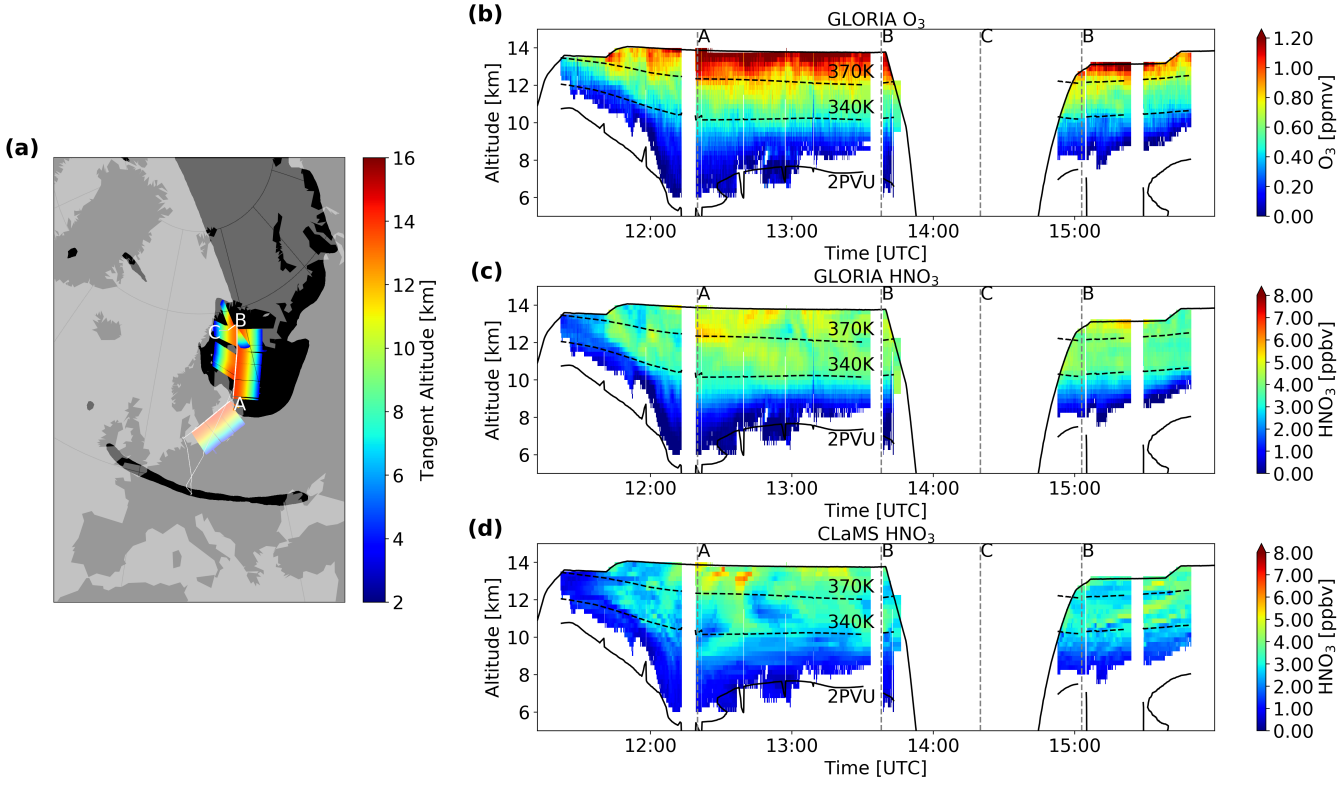

Figure 4. (a) Flight path and vortex filtering according to the Nash criterion at 370 K for flight 21 on 18 March 2016. White line: flight track with characteristic waypoints (A, B, C); light grey shading: areas that are not associated with the polar vortex. Cross-sections of (b) O_3 and (c) HNO_3 distribution derived from GLORIA and (d) HNO_3 distribution simulated by CLaMS for flight 21 on 18 March 2016. Flight altitude (bold black line), characteristic waypoints (A, B, C), 340 K and 370 K potential temperature levels (ECMWF, dashed black lines) and 2 PVU level (ECMWF, black line).

Atmos. Chem. Phys. Discuss., https://doi.org/10.5194/acp-2019-108
Manuscript under review for journal Atmos. Chem. Phys.
Discussion started: 4 March 2019

The flight on 18 March 2016 allowed further sampling of the vortex region at a late state of the winter - about two weeks after the final warming (5-6 March; Manney and Lawrence, 2016). The PV distribution shows a patchy pattern of regions inside the remains of the vortex according to Nash et al. (1996) around Scandinavia, with the GLORIA observations being located partly inside and outside these regions (Fig. 4a).

The measured O_3 distribution (Fig. 4b) shows increasing values with altitude and reaches values of 1.2 ppmv at flight level. Ozone values along the isentropes vary only slightly. The measured HNO_3 distribution (Fig. 4c) shows enhanced values for altitudes higher than 9 km reaching maxima up to 6 ppbv at flight altitude embedded in background values of 2 to 3 ppbv. Filamentation and mixing following the earlier vortex break-up resulted in less spatial variability. However, well-defined local structures originating from nitrification still persisted in this late stage of the winter.

CLaMS (Fig.4d) shows enhanced HNO_3 volume mixing ratios for altitudes higher than 9 km corresponding well with GLORIA observations. Maximum values of locally 6 ppbv are modelled around 12:30 UTC at 13 km. While maximum values are well represented, CLaMS generally underestimates the enhancements and shows a similar spatial variability.

5 Quantification of nitrification of the LMS from December 2015 to January 2016

To quantify nitrification in the LMS from December 2015 to January 2016 HNO_3-O_3-correlations associated with sub-vortex air are analysed for selected flights in this period. GLORIA data points with a calculated relative error larger than 20% are neglected in this study. Here, we use ozone as an approximation of a passive reference tracer, since ozone is well accessible with GLORIA and shows a sufficient vertical gradient in the LMS region. The choice of ozone as a passive tracer is based on the assumption that ozone depletion is small in that period as the air is hardly exposed to sunlight. The model study by Khosrawi et al. (2017) supports this assumption. Two aspects can affect the correlation: 1) Mixing with extra-vortex air masses not affected by nitrification would lead to an underestimation of HNO_3 introduced into the LMS by nitrification and 2) Potential ozone depletion would shift higher HNO_3 mixing ratios to lower ozone values, thus enhancing estimated nitrification.

As correlation scatter plots of measured data for several flights tend to be hard to assess due to the large number of individual points, estimates of relative normalized frequency distributions (RNFD) as described by Eckstein et al. (2017) are used in this study. This method calculates a scaled two dimensional histogram on a volume mixing ratio grid. In this study a grid of 0.070 ppmv O_3 $\times$ 0.35 ppbv HNO_3 is chosen, which is motivated by the total estimated error of the trace gases (Johansson et al., 2018). Besides a clearer presentation of the data points, RNFDs filter out single data points with very high HNO_3 volume mixing ratios. Therefore, in the context of a challenging vortex identification this method offers an additional filter, as single data points that are differing significantly and are erroneously identified as vortex air are filtered out. Here it has to be pointed out that also local non-erroneous points with very high HNO_3 values within the vortex are filtered out applying this method. However, in this study we aim to quantify the overall nitrification of the LMS, while local nitrification is highly inhomogeneous and can reach significantly higher values. The RNFD contour line used for quantification in the following section includes points within 2% of the histograms maximum density.

Atmos. Chem. Phys. Discuss., https://doi.org/10.5194/acp-2019-108
Manuscript under review for journal Atmos. Chem. Phys.
Discussion started: 4 March 2019

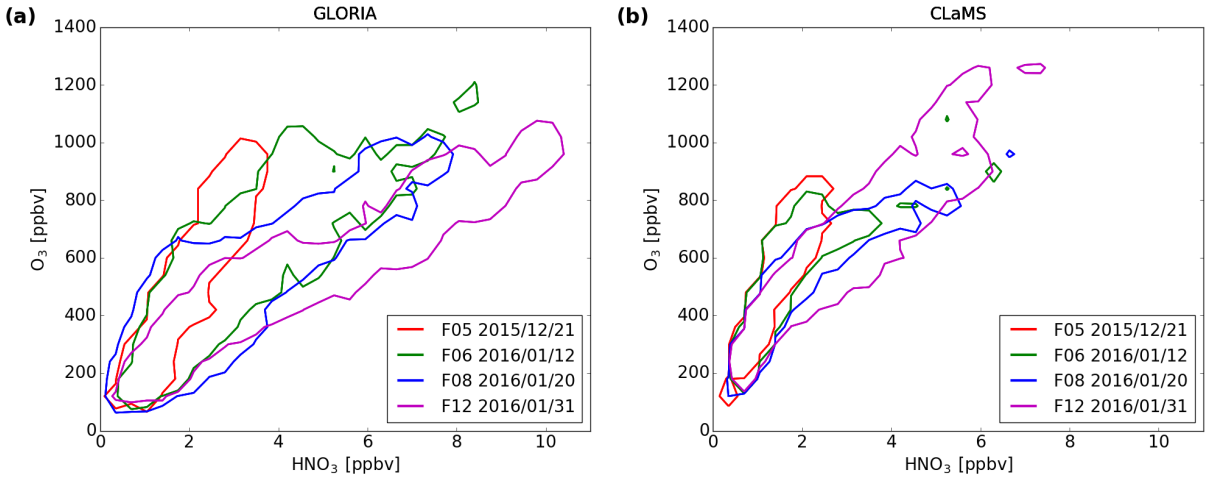

Figure 5. Isolines (contours at 0.02) of the normalized frequency distribution of the O_3-HNO_3-correlation for December 2015 - January 2016 derived from (a) GLORIA measurements and (b) CLaMS simulations.

Fig. 5a depicts the distributions for flights 5, 6, 8 and 12 derived from GLORIA observations. Flight 5 (not discussed here in detail) was carried out on 21 December 2015, at the beginning of the winter, with no significant hints to nitrification. Therefore this flight was chosen as early winter reference. Due to a limited number of points associated with vortex air, non vortex points are also considered here as well.

HNO_3 volume mixing ratios for flight 5 (red) range from 0.25 ppbv to 1.5 ppbv for 0.1 ppmv ozone to 2.8 ppbv to 3.2 ppbv for ozone values of 1 ppmv with an approximately linear relationship. Those values are used as early winter reference. In case of flight 6 (green) enhanced HNO_3 volume mixing ratios up to 7.5 ppbv are observed for ozone values of 1 ppmv. Further a maximum of 8 ppbv is reached for O_3 values of 1.2 ppmv. In comparison to flight 5 enhanced values of HNO_3 are observed for all ozone values. Flight 8 shows a similar enhancement throughout the whole range of ozone mixing ratios observed, reaching maximum HNO_3 volume mixing ratios of 8 ppbv for ozone values of 0.9 ppmv. For flight 12, maximum HNO_3 volume mixing ratios of 10 ppbv are observed for ozone values of 1 ppmv. Altogether, comparing maximum values with the early winter reference, an ongoing nitrification is observed between December 2015 and January 2016 reaching up to 7 ppbv at ozone values of 1 ppmv and 5 ppbv at ozone values of 0.6 ppmv. Johansson (2018b) determined an ozone depletion by 0.15 ppmv at 380 K for ozone values around 1.15 ppmv by the end of January 2016. Assuming this potential ozone depletion of 15% in the LMS during the given time frame, the estimated nitrification would reduce to 5.5 ppbv at 1 ppmv O_3 and 4.0 ppbv at ozone values of 0.6 ppmv. This is a lower limit estimation, especially considering the contrary effect by mixing of non-vortex air masses.

Correlation-based approaches are also suitable for model comparisons. The exact reproduction of complex fine structures by models cannot be expected because of uncertainties in measurements and the model. Differences in the meteorological fields used for modelling, especially the temperature, can result in differing local structures. Since the investigated flights probed a

wide range of the subvortex region, the obtained correlations can be regarded as representative for the (Arctic) sub vortex and allow for a comparison between model and measurement. We point out that observed differences in RNFDs can be caused by an inaccurate representation of processes influencing both, HNO_3 as well as O_3 volume mixing ratios.

The distributions simulated by CLaMS are shown in Fig. 5b. For flight 5 HNO_3 volume mixing ratios between 0.5 and 2.5 ppbv are observed with maximum ozone volume mixing ratios of 0.85 ppmv. Flight 6 shows enhanced HNO_3 volume mixing ratios of up to 3.5 ppbv for O_3 values up to 0.8 ppmv and patches of further enhanced HNO_3 for ozone values between 0.8 ppmv and 1 ppmv. CLaMS models a further enhancement for flight 8 reaching up to 5.5 ppbv HNO_3 for ozone values of 0.8 ppmv with a patch reaching 6.5 ppbv at 0.9 ppmv O_3. Flight 12 displays highest HNO_3 volume mixing ratios of about 6.5 ppbv for ozone values between 0.9 ppmv and 1.2 ppmv. One patch reaches 7 ppbv.

Beneath 0.3 ppmv O_3 hardly any enhancement is observed over the duration of the flights. Overall, CLaMS is able to reproduce the general enhancement of HNO_3 during the winter leading to a nitrification of up to 4 ppbv for ozone values of 0.8 to 1 ppmv, which is by 3 ppbv HNO_3 lower than the GLORIA observations.

6 Comparison of GLORIA results with CLaMS sensitivity simulations

Four sensitivity simulations have been performed in order to investigate processes and aspects that have not been represented in the model so far. These sensitivity simulations were performed based on assumptions concerning particle formation and shape. Besides the formation of NAT on ice particles, ice can possibly accumulate on NAT particles (Voigt et al., 2018) resulting in larger particles with an enhanced settling velocity. Therefore in the 'ice settling' simulation a 1.5 times enhanced settling velocity is applied if the saturation ratio of ice, S_{Ice}, is larger than 1.2. Since NAT formation is temperature dependent a sensitivity simulation is performed with a global temperature offset of 1 K. Particle growth in CLaMS is based on the assumption of growth rates of spherical particles. However, Woiwode et al. (2016) found indications for highly aspherical particles with an enhanced surface compared to spherical particles of the same volume. Since the HNO_3 uptake depends on the surface, a faster particle growth would occur. A 1.5 times enhanced particle growth was implemented in the 'aspherical particle' simulation. Changes in settling velocities due to different shapes have not been taken into account here. Several studies suggest a connection between orographically induced gravity waves and NAT formation (Davies et al., 2005; Carslaw et al., 1998; Höpfner et al., 2006). However small scale temperature fluctuations are not resolved by ERA interim temperatures. Therefore, artificial fluctuations according to (Tritscher et al., 2018) have been added in the 'temperature fluctuations' simulation.

The comparison is based on the RNFDs depicted for the individual flights in Fig. 6. As an example, the cross-sections of the different simulations (Fig. 7) for flight 6 have been analysed as well. The cross-sections for flights 8, 12 and 21 can be found in the appendix (Fig. A1, A2, A3).

6.1 Flight 6 on 12 January 2016

The sensitivity simulations' cross-sections for flight 6 are shown in Fig. 7c-f together with the GLORIA measurement in Fig. 7a and the reference simulation in Fig. 7b. The 'ice settling' simulation (Fig. 7c) delivers virtually identical results as the reference

Atmos. Chem. Phys. Discuss., https://doi.org/10.5194/acp-2019-108
Manuscript under review for journal Atmos. Chem. Phys.
Discussion started: 4 March 2019

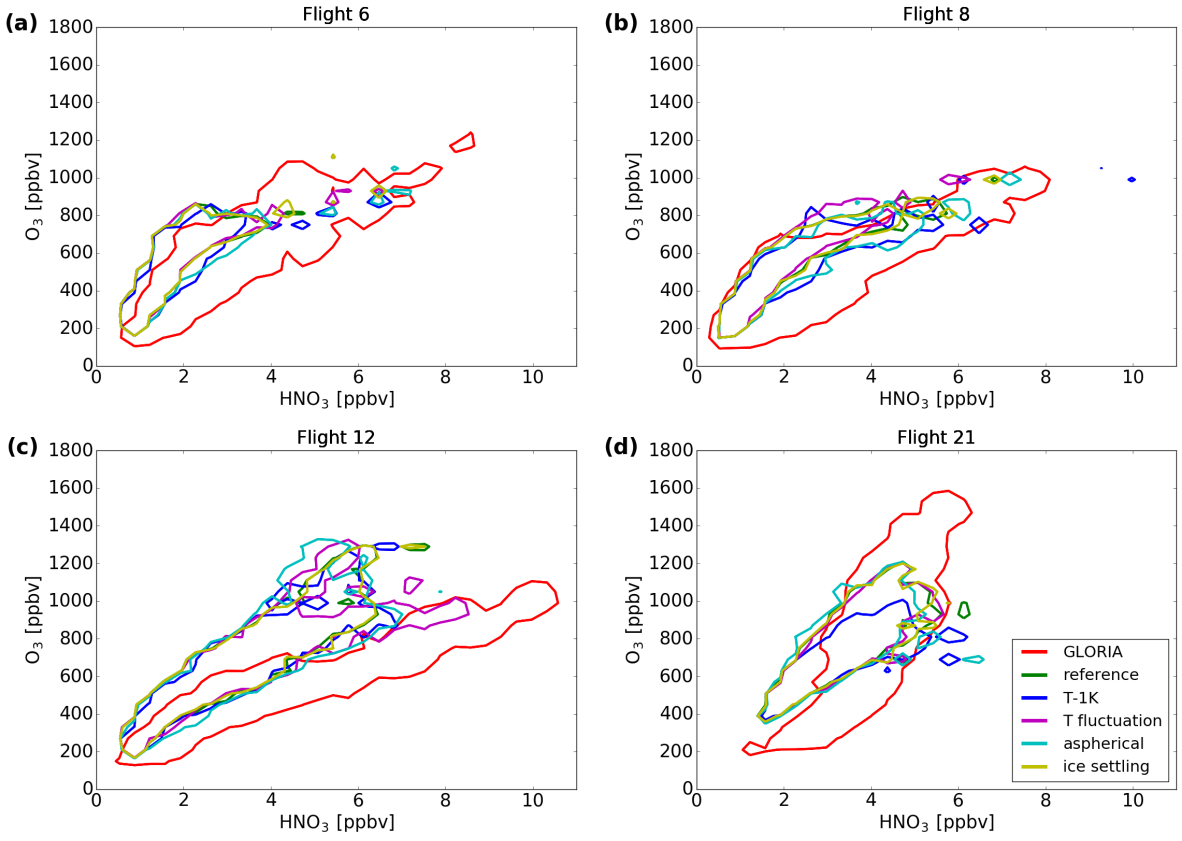

Figure 6. Isolines (contours at 0.02) of the normalized frequency distribution of the O_3-HNO_3-correlation for (a) flight 6 on 12 January 2016, (b) flight 8 on 20 January 2016, (c) flight 12 on 31 January 2016, (d) flight 21 on 18 March 2016 derived from GLORIA measurements (red) and CLaMS simulations.

simulation for this flight. This is also observed in the RNFD depicted in Fig. 6a. The 'aspherical particle' case (Fig. 7e) shows a strengthening of existing maxima. The RNFD supports this observation and shows enhanced values down to lower altitudes than the reference simulation. Further, the band like structure observed by GLORIA around 12:40 UTC is more pronounced in the cross-section of this simulation. The absolute values there are still underestimated. The 'T-1K' simulation (Fig. 7f) shows a maximized area of enhanced values that are reaching further down. This enhancement at lower altitudes also appears in the RNFD. Moreover, the band-like structure around 12:40 UTC is more developed than in the reference simulation. For the 'temperature fluctuation' simulation (Fig. 7d) slightly lower enhancements are found. However, the overall structure in the RNFD is similar to the reference simulation.

Atmos. Chem. Phys. Discuss., https://doi.org/10.5194/acp-2019-108
Manuscript under review for journal Atmos. Chem. Phys.
Discussion started: 4 March 2019

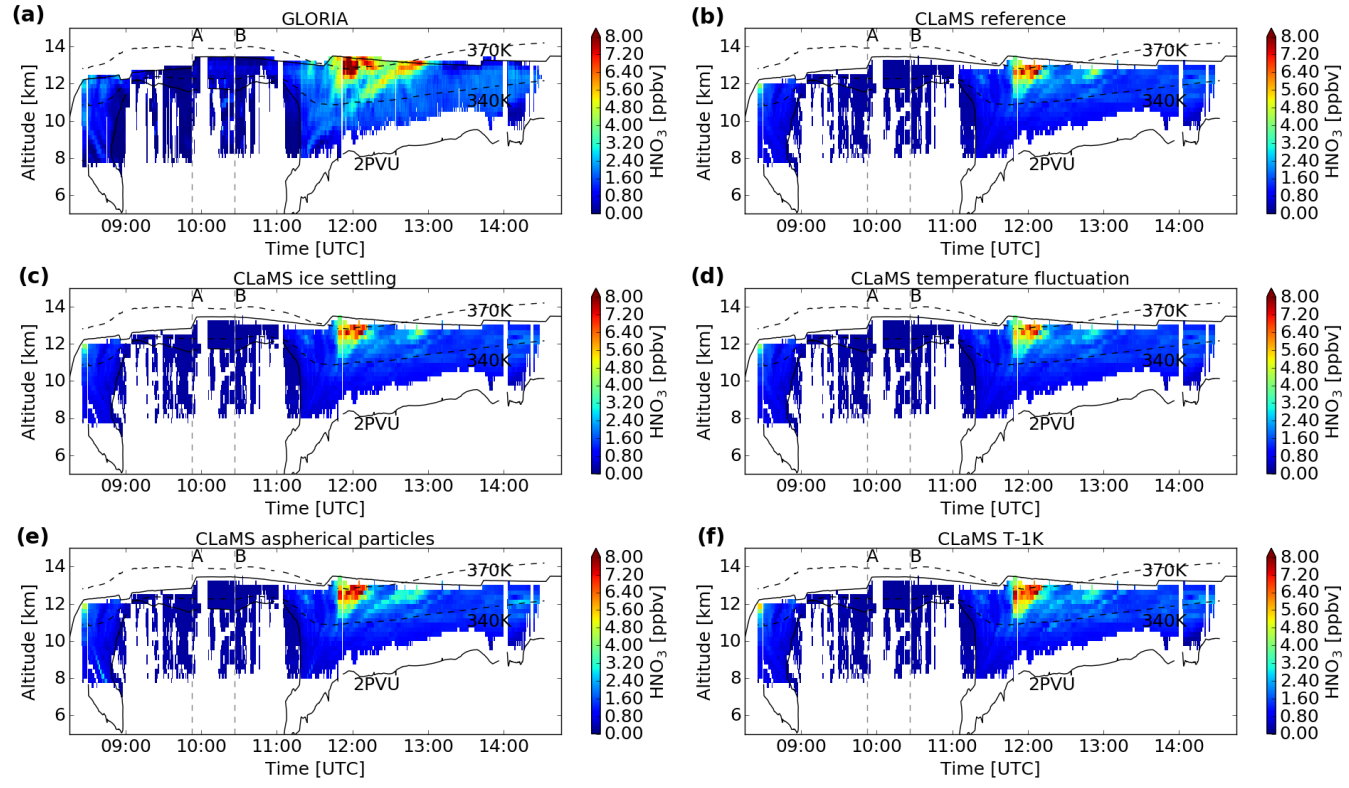

Figure 7. Cross-sections of HNO_3 volume mixing ratio distribution for flight 6 on 12 January 2016 derived by GLORIA (a) and modelled by the CLaMS reference simulation (b) and sensitivity simulations considering (c) ice formation on NAT particles, (d) temperature fluctuations, (e) growth rates of aspherical particles, (f) 1K global temperature offset. Flight altitude (bold black line), characteristic waypoints (A, B, C), 340 K and 370 K potential temperature levels (ECMWF, dashed black lines) and 2 PVU level (ECMWF, black line).

6.2 Flight 8 on 20 January 2016

For flight 8, relative normalized frequency distributions are shown in Fig. 6b for all CLaMS simulations together with the GLORIA result. The 'ice settling' simulation simulates nearly identical structures as the reference simulation. For 'T-1K', enhanced HNO_3 volume mixing ratios are observed down to lower O_3 volume mixing ratios compared to the reference simulation, but are still not reaching down to the ozone values noticed by GLORIA. The RNFD for this simulation shows best agreement with the GLORIA observations. High HNO_3 volume mixing ratios are still underestimated here. The 'aspherical particle' simulation results in enhanced values observed down to lower altitudes than for the reference simulation. The RNFD results in higher HNO_3 values compared to the reference. However, there are also indications for points with lower values than for the reference. For the 'temperature fluctuation' case lower HNO_3 volume mixing ratios are observed.

Atmos. Chem. Phys. Discuss., https://doi.org/10.5194/acp-2019-108
Manuscript under review for journal Atmos. Chem. Phys.
Discussion started: 4 March 2019


Atmospheric Chemistry and Physics Discussions

6.3 Flight 12 on 31 January 2016

RNFDs for all sensitivity simulations are shown in Fig. 6c. The 'ice settling' case for flight 12 shows virtually identical results as the reference simulation. For the 'temperature offset' simulation higher maximum values are modelled at O_3 volume mixing ratios between 600 and 900 ppbv. However, there are indications for lower volume mixing ratios for some points as well. For the 'temperature fluctuation' simulation, a significant enhancement of maximum HNO_3 values is found reaching maximum values of 8 ppbv for ozone volume mixing ratios of 900 ppbv. This RNFD shows the best agreement with the GLORIA observations for this flight. However, even though the lower branch is consistent with GLORIA, an upper branch with values lower than the reference simulation and far lower than GLORIA exists. The 'aspherical particle' simulation shows a distribution with higher spread and values partly higher, partly lower, than for the reference case.

6.4 Flight 21 on 18 March 2016

For flight 21 the RNFDs are depicted in Fig. 6d. The 'ice settling' simulation, as well as the 'temperature fluctuation' simulation, shows only small differences compared to the reference simulation. In the 'aspherical particle' simulation enhanced values appear at slightly lower O_3 volume mixing rations than for the reference simulation. There are also indications for points with lower HNO_3 values. Generally, the different CLaMS simulations are similar in their structure, but the simulations differ significantly from the GLORIA results. The only simulation clearly deteriorating is the 'T-1K' case. For this flight none of the CLaMS simulations is able to reproduce the high ozone volume mixing ratios observed by GLORIA, which is possibly caused by weaker subsidence in the model. Further, lower absolute HNO_3 values might occur due to stronger mixing in CLaMS.

7 Discussion and Conclusion

Nitrification of the LMS in the Arctic winter 2015/16 was analysed based on GLORIA measurements during the PGS campaign. Vertical cross sections of HNO_3 volume mixing ratios for several flights throughout the winter show complex fine scale structures and enhanced values at altitudes down to 9 km. For flight 6 in mid-January single profiles with HNO_3 volume mixing ratios exceeding 8 ppbv were observed. Flight 8 on 20 January 2016 was carried out under cold conditions with PSC observations at flight altitude. For this flight, band-like structures of enhanced HNO_3 volume mixing ratios are observed that most likely indicate defined regions where settled HNO_3-containing particles recently sublimated. This is supported by simultaneous in situ observations of HNO_3-containing particles. The net effect of proceeding nitrification and dynamical processes in the LMS is observed for flight 12 at the end of January with a pronounced pattern of enhanced HNO_3 volume mixing ratios well exceeding 10 ppbv. Nitrified filaments with HNO_3 volume mixing ratios up to 6 ppbv persist until flight 21 in March 2016. While cross-sections provide an insight on the local nitrifications spatial and structural influence for selected flights, the extent of overall nitrification has been quantified based on HNO_3-O_3-correlations. Nitrification reached an extent of up to 7 ppbv at ozone values of 1 ppmv ($\theta \approx 370$ K) and up to 5 ppbv at ozone values of 0.6 ppmv ($\theta \approx 350$ K). A conservative correction, assuming a 15 % ozone loss on the correlations would reduce these numbers to 5.5 ppbv and 4 ppbv, respectively.

The comparison of GLORIA observations with the chemistry transport model CLaMS confirm the model's ability to reproduce nitrification of the LMS. Large-scale structures are reproduced by the model that also resolves complex fine structures, although differing from measured patterns. CLaMS predominantly underestimates the enhanced values observed by GLORIA. Strongly enhanced values are found less frequently in the simulation and are limited to narrow regions. Further, modelled HNO_3 enhancements reach less far down on 12 and 20 January 2016 when compared with GLORIA. The CLaMS simulations result in a weaker nitrification of up to 4 ppbv for the period of December to January for ozone mixing ratios between 0.8 ppmv to 1 ppmv, which is by ∼3 ppbv lower than observed by GLORIA. For flight 21 in March, CLaMS underestimates the observed ozone volume mixing ratios, potentially indicating insufficient subsidence and stronger mixing in the model (Johansson, 2018b). Sensitivity studies with CLaMS considering i) ice formation on NAT particles, ii) a 1 K global temperature offset, iii) growth rates of aspherical particles or iv) temperature fluctuations were performed. While the 'ice formation' simulation shows only slight differences, the other cases show distinct differences for selected flights. The 'temperature fluctuation' simulation provides improved agreement for the flight on 31 January 2016, but also worsens the results for the flight on 20 January 2016. The 'T-1K' simulation improves the results for all flights in January, but deteriorates the results for the flight in the late winter on 18 March 2016. This shows the sensitivity of the simulation results on temperature. Potentially, a higher resolution in time and space would result in more realistic temperature fluctuations and could improve the simulations. The 'aspherical particle' case shows slightly more pronounced improvements for the flights in mid-January. Even though the sensitivity simulations generally improve the results, significant differences between model and measurements remain. The sensitivity simulations suggest that particle microphysics play a significant role for LMS nitrification in January. Increasing discrepancies from the observations towards the end of the winter are attributed to simulated air subsidence, transport and mixing processes.

Several studies investigated nitrification in previous cold winters, although mainly with a focus on higher altitudes. For the Arctic winter 2002/03 Grooß et al. (2005) modelled a nitrification of less than 1 ppbv for potential temperatures lower than 360 K. For the Arctic winter 2004/05, Dibb et al. (2006) observe nitrification of up to 3 ppbv for potential temperatures between 360 and 340 K. Jin et al. (2006) report an average nitrification of less than 2 ppbv for potential temperatures lower than 370 K for the same winter. Further, during the Arctic winter 2009/10 (Grooß et al., 2014) modelled a nitrification of less than 1 ppbv for potential temperatures lower than 360 K, while (Woiwode et al., 2014) found no significant indications for nitrification below 370 K. Since Arctic winters might show a tendency towards colder stratospheric temperatures (Rex et al., 2006), disturbances of the LMS NO_y budget by nitrification are likely becoming more frequent. The measurements obtained by GLORIA during the POLSTRACC campaign document in detail a strong impact of nitrification on the LMS during an entire Arctic winter for the first time.

Data availability. The discussed GLORIA data set is available at the HALO database at https://halo-db.pa.op.dlr.de/. NASA MERRA2 reanalysis data is available at https://disc.gsfc.nasa.gov/.

Atmos. Chem. Phys. Discuss., https://doi.org/10.5194/acp-2019-108
Manuscript under review for journal Atmos. Chem. Phys.
Discussion started: 4 March 2019

Atmospheric Chemistry and Physics Discussions

Appendix A

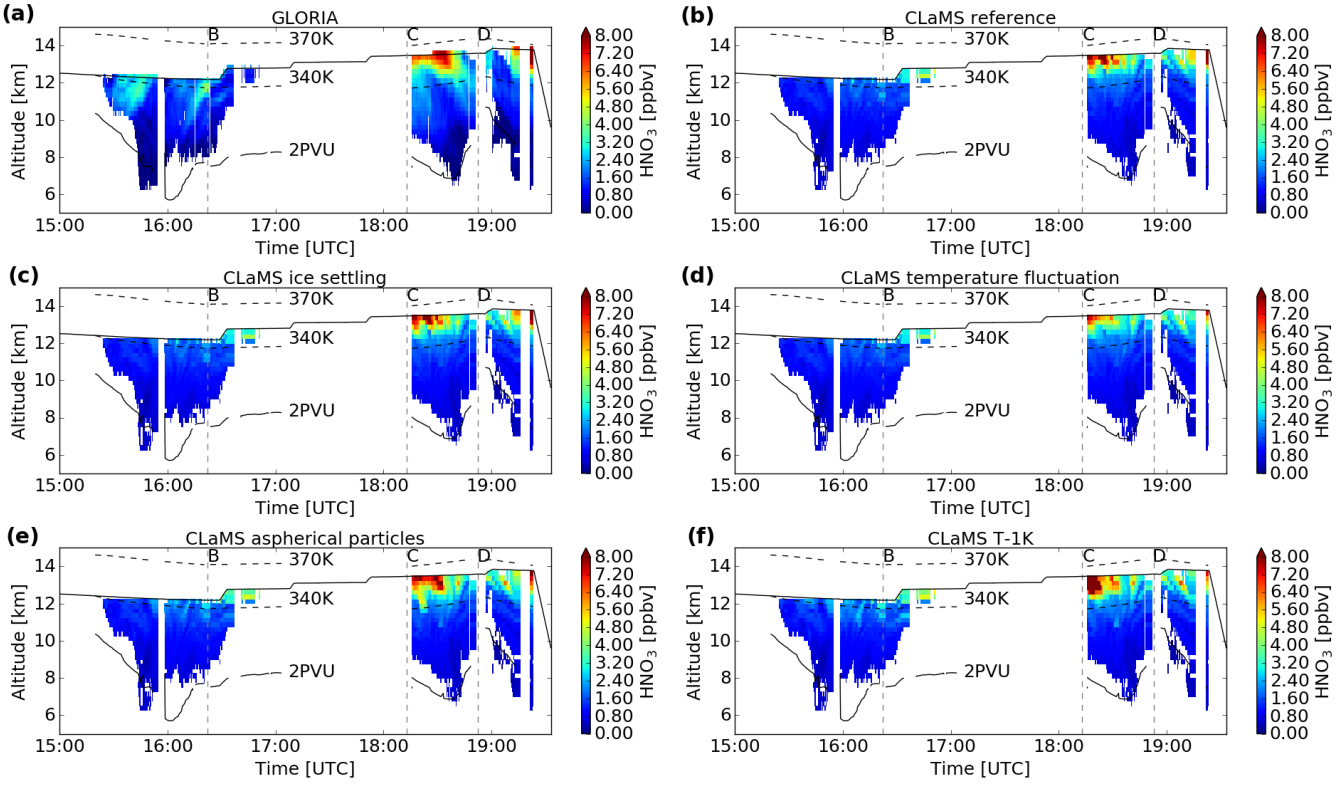

Figure A1. Cross-sections of HNO_3 volume mixing ratio distribution for flight 8 on 20 January 2016 derived by GLORIA (a) and modelled by the CLaMS reference simulation (b) and sensitivity simulations considering (c) ice formation on NAT particles, (d) temperature fluctuations, (e) growth rates of aspherical particles, (f) 1K global temperature offset. Flight altitude (bold black line), characteristic waypoints (), 340 K and 370 K potential temperature levels (ECMWF, dashed black lines) and 2 PVU level (ECMWF, black line).

Author contributions. MB conducted the analysis and interpretation of GLORIA level-2 data and model simulations and prepared the manuscript with contributions from all co-authors. JUG performed the CLaMS model simulations. WW, SJ, JU performed the level-1 and -2 analysis of GLORIA data. MH contributed to the GLORIA data analysis and interpretation. FFV, PP operated the GLORIA instrument during the PGS campaign. HO, BMS coordinated the PGS field campaign. HZ provided the particle HNO3 data. PB contributed to the interpretation and the manuscript preparation.

Competing interests. The authors declare that they have no conflict of interest.

Atmos. Chem. Phys. Discuss., https://doi.org/10.5194/acp-2019-108
Manuscript under review for journal Atmos. Chem. Phys.
Discussion started: 4 March 2019

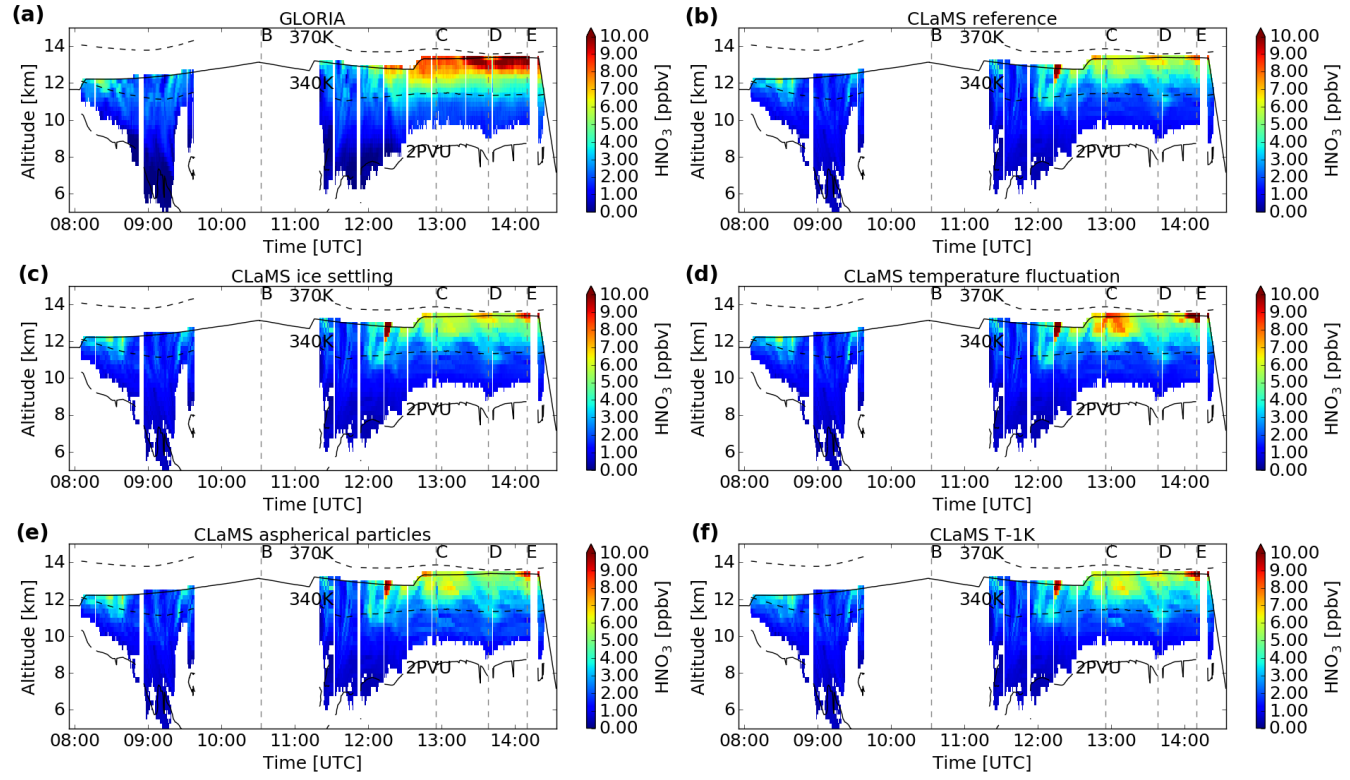

Figure A2. Cross-sections of HNO_3 volume mixing ratio distribution for flight 12 on 31 January 2016 derived by GLORIA (a) and modelled by the CLaMS reference simulation (b) and sensitivity simulations considering (c) ice formation on NAT particles, (d) temperature fluctuations, (e) growth rates of aspherical particles, (f) 1K global temperature offset. Flight altitude (bold black line), characteristic waypoints (), 340 K and 370 K potential temperature levels (ECMWF, dashed black lines) and 2 PVU level (ECMWF, black line). Please note the changed colorbar compared to Figs. 7,A1,A3.

Acknowledgements. We thank the PGS coordination team and the DLR-FX for successfully conducting the field campaign. The results are based on the efforts of all members of the GLORIA team, including the technology institutes ZEA-1 and ZEA-2 at Forschungszentrum Jülich. We thank NASA for providing their MERRA2 meteorological reanalysis data set. We acknowledge the computing time for the CLaMS 5 simulations granted on the supercomputer JURECA at Jülich Supercomputing Centre (JSC) under the VSR project ID JICG11. This work was supported by the German Research Foundation (Deutsche Forschungsgemeinschaft, DFG Priority Program SPP 1294). S. Johansson has received funding from the European Community's Seventh Framework Programme (FP7/2007-2013) under grant agreement 603557. Further support was received by the German research initiative ROMIC (Role of the Middle Atmosphere in Climate) and by the German Ministry of Research and Education (BMBF) project "Investigation of the life cycle of gravity waves" (GW-LCYCLE, subproject 2, 01LG1206B). We acknowledge support by the Deutsche Forschungsgemeinschaft and the Open Access Publishing Fund of the Karlsruhe Institute of Technology.

Atmos. Chem. Phys. Discuss., https://doi.org/10.5194/acp-2019-108
Manuscript under review for journal Atmos. Chem. Phys.
Discussion started: 4 March 2019

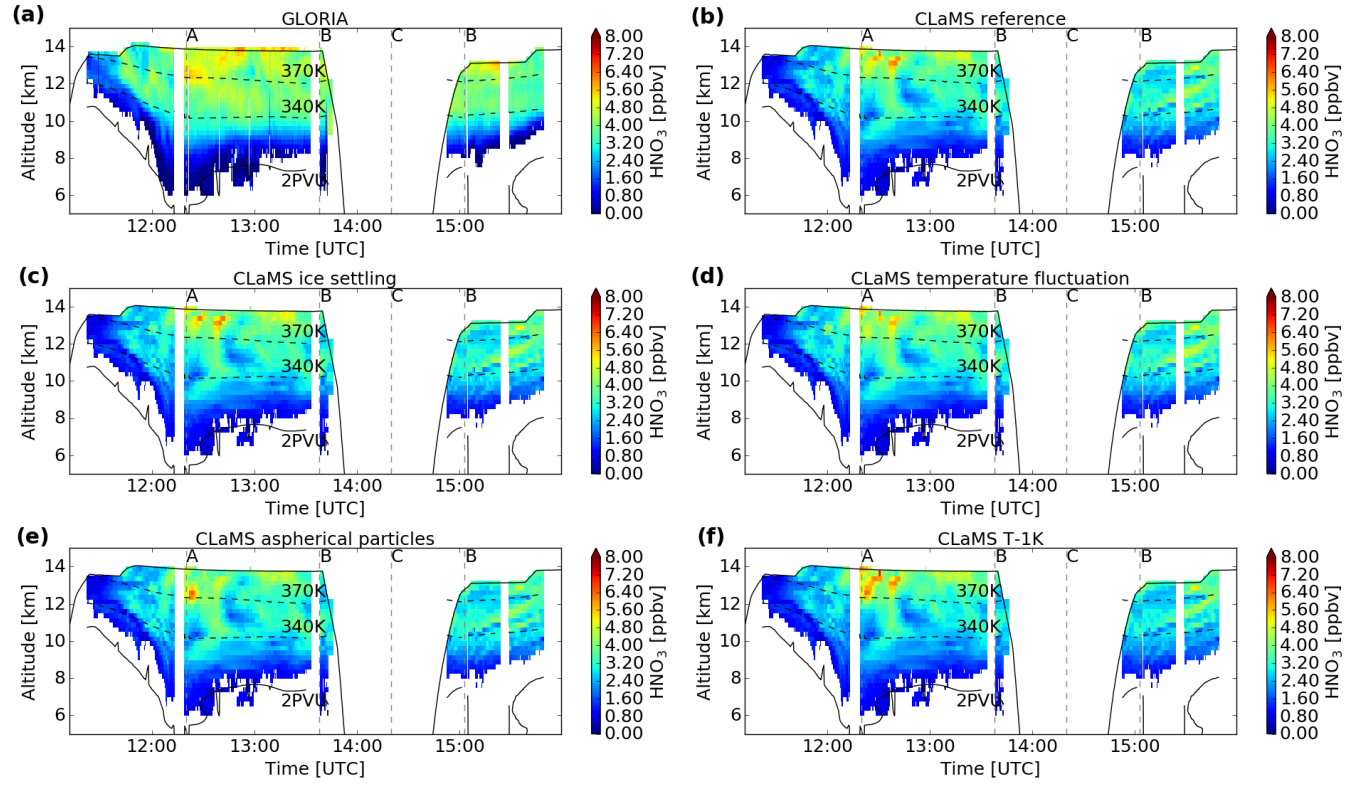

Figure A3. Cross-sections of HNO_3 volume mixing ratio distribution for flight 21 on 18 March 2016 derived by GLORIA (a) and modelled by the CLaMS reference simulation (b) and sensitivity simulations considering (c) ice formation on NAT particles, (d) temperature fluctuations, (e) growth rates of aspherical particles, (f) 1K global temperature offset. Flight altitude (bold black line), characteristic waypoints (A, B, C), 340 K and 370 K potential temperature levels (ECMWF, dashed black lines) and 2 PVU level (ECMWF, black line).

References

Carslaw, K. S.: A vortex-scale simulation of the growth and sedimentation of large nitric acid hydrate particles, Journal of Geophysical Research, 107, https://doi.org/10.1029/2001JD000467, 2002.

Carslaw, K. S., Wirth, M., Tsias, A., Luo, B. P., Dörnbrack, A., Leutbecher, M., Volkert, H., Renger, W., Bacmeister, J. T., and Peter, T.: Particle microphysics and chemistry in remotely observed mountain polar stratospheric clouds, Journal of Geophysical Research: Atmospheres, 103, 5785–5796, https://doi.org/10.1029/97JD03626, 1998.

Davies, S., Mann, G. W., Carslaw, K. S., Chipperfield, M. P., Kettleborough, J. A., Santee, M. L., Oelhaf, H., Wetzel, G., Sasano, Y., and Sugita, T.: 3-D microphysical model studies of Arctic denitrification: Comparison with observations, Atmospheric Chemistry and Physics, 5, 3093–3109, https://doi.org/10.5194/acp-5-3093-2005, 2005.

Dee, D. P., Uppala, S. M., Simmons, A. J., Berrisford, P., Poli, P., Kobayashi, S., Andrae, U., Balmaseda, M. A., Balsamo, G., Bauer, P., Bechtold, P., Beljaars, A. C. M., van de Berg, L., Bidlot, J., Bormann, N., Delsol, C., Dragani, R., Fuentes, M., Geer, A. J., Haimberger, L., Healy, S. B., Hersbach, H., Hólm, E. V., Isaksen, L., Kållberg, P., Köhler, M., Matricardi, M., McNally, A. P., Monge-Sanz,

B. M., Morcrette, J.-J., Park, B.-K., Peubey, C., de Rosnay, P., Tavolato, C., Thépaut, J.-N., and Vitart, F.: The ERA-Interim reanalysis: configuration and performance of the data assimilation system, Quarterly Journal of the Royal Meteorological Society, 137, 553–597, https://doi.org/10.1002/qj.828, https://rmets.onlinelibrary.wiley.com/doi/abs/10.1002/qj.828, 2011.

Dibb, J. E., Scheuer, E., Avery, M., Plant, J., and Sachse, G.: In situ evidence for renitrification in the Arctic lower stratosphere during the polar aura validation experiment (PAVE), Geophysical Research Letters, 33, https://doi.org/10.1029/2006GL026243, https://agupubs.onlinelibrary.wiley.com/doi/abs/10.1029/2006GL026243, 2006.

Dunkerton, T. J. and Delisi, D. P.: Evolution of potential vorticity in the winter stratosphere of January-February 1979, Journal of Geophysical Research, 91, 1199, https://doi.org/10.1029/JD091iD01p01199, 1986.

Eckstein, J., Ruhnke, R., Pfahl, S., Christner, E., Dyroff, C., Reinert, D., Rieger, D., Schneider, M., Schröter, J., Zahn, A., and Braesicke, P.: From climatological to small scale applications: Simulating water isotopologues with ICON-ART-Iso (version 2.1), Geoscientific Model Development Discussions, accepted for GMD, pp. 1–31, https://doi.org/10.5194/gmd-2017-280, 2017.

Engel, I., Luo, B. P., Pitts, M. C., Poole, L. R., Hoyle, C. R., Grooß, J.-U., Dörnbrack, A., and Peter, T.: Heterogeneous formation of polar stratospheric clouds – Part 2: Nucleation of ice on synoptic scales, Atmospheric Chemistry and Physics, 13, 10 769–10 785, https://doi.org/10.5194/acp-13-10769-2013, https://www.atmos-chem-phys.net/13/10769/2013/, 2013.

Fahey, D. W., Kelly, K. K., Kawa, S. R., Tuck, A. F., Loewenstein, M., Chan, K. R., and Heidt, L. E.: Observations of denitrification and dehydration in the winter polar stratospheres, Nature, 344, 321– 324, https://doi.org/http://dx.doi.org/10.1038/344321a0, 1990.

Fischer, H., Waibel, A. E., Welling, M., Wienhold, F. G., Zenker, T., Crutzen, P. J., Arnold, F., Bürger, V., Schneider, J., Bregman, A., Lelieveld, J., and Siegmund, P. C.: Observations of high concentrations of total reactive nitrogen (NO y) and nitric acid (HNO3) in the lower Arctic stratosphere during the Stratosphere-Troposphere Experiment by Aircraft Measurements (STREAM) II campaign in February 1995, Journal of Geophysical Research: Atmospheres, 102, 23 559–23 571, https://doi.org/10.1029/97JD02012, https://agupubs.onlinelibrary.wiley.com/doi/abs/10.1029/97JD02012, 1997.

Fischer, H., Birk, M., Blom, C., Carli, B., Carlotti, M., von Clarmann, T., Delbouille, L., Dudhia, A., Ehhalt, D., Endemann, M., Flaud, J. M., Gessner, R., Kleinert, A., Koopman, R., Langen, J., López-Puertas, M., Mosner, P., Nett, H., Oelhaf, H., Perron, G., Remedios, J., Ridolfi, M., Stiller, G., and Zander, R.: MIPAS: an instrument for atmospheric and climate research, Atmospheric Chemistry and Physics, 8, 2151–2188, https://doi.org/10.5194/acp-8-2151-2008, https://www.atmos-chem-phys.net/8/2151/2008/, 2008.

Friedl-Vallon, F., Gulde, T., Hase, F., Kleinert, A., Kulessa, T., Maucher, G., Neubert, T., Olschewski, F., Piesch, C., Preusse, P., Rongen, H., Sartorius, C., Schneider, H., Schönfeld, A., Tan, V., Bayer, N., Blank, J., Dapp, R., Ebersoldt, A., Fischer, H., Graf, F., Guggenmoser, T., Höpfner, M., Kaufmann, M., Kretschmer, E., Latzko, T., Nordmeyer, H., Oelhaf, H., Orphal, J., Riese, M., Schardt, G., Schillings, J., Sha, M. K., Suminska-Ebersoldt, O., and Ungermann, J.: Instrument concept of the imaging Fourier transform spectrometer GLORIA, Atmospheric Measurement Techniques, 7, 3565–3577, https://doi.org/10.5194/amt-7-3565-2014, 2014.

Gettelman, A., Hoor, P., Pan, L. L., Randel, W. J., Hegglin, M. I., and Birner, T.: THE EXTRATROPICAL UPPER TROPOSPHERE AND LOWER STRATOSPHERE, Reviews of Geophysics, 49, https://doi.org/10.1029/2011RG000355, https://agupubs.onlinelibrary.wiley.com/doi/abs/10.1029/2011RG000355, 2011.

Grooß, J.-U., Günther, G., Müller, R., Konopka, P., Bausch, S., Schlager, H., Voigt, C., Volk, C. M., and Toon, G. C.: Simulation of denitrification and ozone loss for the Arctic winter 2002/2003, Atmospheric Chemistry and Physics, 5, 1437–1448, https://doi.org/10.5194/acp-5-1437-2005, 2005.

Grooß, J.-U., Engel, I., Borrmann, S., Frey, W., Günther, G., Hoyle, C. R., Kivi, R., Luo, B. P., Molleker, S., Peter, T., Pitts, M. C., Schlager, H., Stiller, G., Vömel, H., Walker, K. A., and Müller, R.: Nitric acid trihydrate nucleation and denitrification in the Arctic stratosphere, Atmospheric Chemistry and Physics, 14, 1055–1073, https://doi.org/10.5194/acp-14-1055-2014, 2014.

Höpfner, M., Larsen, N., Spang, R., Luo, B. P., Ma, J., Svendsen, S. H., Eckermann, S. D., Knudsen, B., Massoli, P., Cairo, F., Stiller, G., v. Clarmann, T., and Fischer, H.: MIPAS detects Antarctic stratospheric belt of NAT PSCs caused by mountain waves, Atmospheric Chemistry and Physics, 6, 1221–1230, https://doi.org/10.5194/acp-6-1221-2006, https://www.atmos-chem-phys.net/6/1221/2006/, 2006.

Hoyle, C. R., Engel, I., Luo, B. P., Pitts, M. C., Poole, L. R., Groo, J.-U., and Peter, T.: Heterogeneous formation of polar stratospheric clouds - Part 1: Nucleation of nitric acid trihydrate (NAT), Atmospheric Chemistry and Physics, 13, 9577–9595, https://doi.org/10.5194/acp-13-9577-2013, 2013.

Höpfner, M., Blom, C. E., Echle, G., Glatthor, N., Hase, F., Stiller, G. P., Karlsruhe, F., and Karlsruhe, U.: G.: Retrieval simulations for MIPAS-STR measurements, in: Hrsg.] IRS 2000: Current Problems in Atmospheric Radiation; Proc.of the Internat. Radiation Symp., St.Petersburg, DEEPAK Publ, 2001.

Jin, J. J., Semeniuk, K., Manney, G. L., Jonsson, A. I., Beagley, S. R., McConnell, J. C., Rinsland, C. P., Boone, C. D., Walker, K. A., and Bernath, P. F.: Denitrification in the Arctic winter 2004/2005: Observations from ACE-FTS, Geophysical Research Letters, 33, L15S01, https://doi.org/10.1029/2006GL027687, 2006.

Johansson, S., Woiwode, W., Höpfner, M., Friedl-Vallon, F., Kleinert, A., Kretschmer, E., Latzko, T., Orphal, J., Preusse, P., Ungermann, J., Santee, M. L., Jurkat-Witschas, T., Marsing, A., Voigt, C., Giez, A., Krämer, M., Rolf, C., Zahn, A., Engel, A., Sinnhuber, B.-M., and Oelhaf, H.: Airborne limb-imaging measurements of temperature, HNO_3, O_3, $ClONO_2$, H_2O and CFC-12 during the Arctic winter 2015/2016: characterization, in situ validation and comparison to Aura/MLS, Atmospheric Measurement Techniques, 11, 4737–4756, https://doi.org/10.5194/amt-11-4737-2018, https://www.atmos-meas-tech.net/11/4737/2018/, 2018.

Johansson, S. e. a.: Unusual chlorine partitioning in the 2015/16 Arctic winter lowermost stratosphere: Observations and simulations, Atmospheric Chemistry and Physics Discussions, 2018, 2018b.

Khosrawi, F., Urban, J., Pitts, M. C., Voelger, P., Achtert, P., Kaphlanov, M., Santee, M. L., Manney, G. L., Murtagh, D., and Fricke, K.-H.: Denitrification and polar stratospheric cloud formation during the Arctic winter 2009/2010, Atmospheric Chemistry and Physics, 11, 8471–8487, https://doi.org/10.5194/acp-11-8471-2011, 2011.

Khosrawi, F., Kirner, O., Sinnhuber, B.-M., Johansson, S., Höpfner, M., Santee, M. L., Froidevaux, L., Ungermann, J., Ruhnke, R., Woiwode, W., Oelhaf, H., and Braesicke, P.: Denitrification, dehydration and ozone loss during the Arctic winter 2015/2016, Atmospheric Chemistry and Physics Discussions, pp. 1–33, https://doi.org/10.5194/acp-2017-503, 2017.

Kim, Y., Choi, W., Lee, K., Park, J. H., Massie, S. T., Sasano, Y., Nakajima, H., and Yokota, T.: Polar stratospheric clouds observed by the ILAS-II in the Antarctic region: Dual compositions and variation of compositions during June to August of 2003, Journal of Geophysical Research: Atmospheres, 111, https://doi.org/10.1029/2005JD006445, https://agupubs.onlinelibrary.wiley.com/doi/abs/10.1029/2005JD006445, 2006.

Kleinert, A., Friedl-Vallon, F., Guggenmoser, T., Höpfner, M., Neubert, T., Ribalda, R., Sha, M. K., Ungermann, J., Blank, J., Ebersoldt, A., Kretschmer, E., Latzko, T., Oelhaf, H., Olschewski, F., and Preusse, P.: Level 0 to 1 processing of the imaging Fourier transform spectrometer GLORIA: generation of radiometrically and spectrally calibrated spectra, Atmospheric Measurement Techniques, 7, 4167–4184, https://doi.org/10.5194/amt-7-4167-2014, https://www.atmos-meas-tech.net/7/4167/2014/, 2014.

Krause, J., Hoor, P., Engel, A., Plöger, F., Grooß, J.-U., Bönisch, H., Keber, T., Sinnhuber, B.-M., Woiwode, W., and Oelhaf, H.: Mixing and ageing in the polar lower stratosphere in winter 2015–2016, Atmospheric Chemistry and Physics, 18, 6057–6073, https://doi.org/10.5194/acp-18-6057-2018, https://www.atmos-chem-phys.net/18/6057/2018/, 2018.

Manney, G. L. and Lawrence, Z. D.: The major stratospheric final warming in 2016: Dispersal of vortex air and termination of Arctic chemical ozone loss, Atmospheric Chemistry and Physics, 16, 15 371–15 396, https://doi.org/10.5194/acp-16-15371-2016, 2016.

Manney, G. L., Zurek, R. W., O'Neill, A., and Swinbank, R.: On the Motion of Air through the Stratospheric Polar Vortex, Journal of the Atmospheric Sciences, 51, 2973–2994, https://doi.org/10.1175/1520-0469(1994)051<2973:OTMOAT>2.0.CO;2, 1994.

Matthias, V., Dörnbrack, A., and Stober, G.: The extraordinarily strong and cold polar vortex in the early northern winter 2015/2016, Geophysical Research Letters, 43, 12,287–12,294, https://doi.org/10.1002/2016GL071676, 2016.

McKenna, D. S.: A new Chemical Lagrangian Model of the Stratosphere (CLaMS) 1. Formulation of advection and mixing, Journal of Geophysical Research, 107, 1435, https://doi.org/10.1029/2000JD000114, 2002a.

McKenna, D. S.: A new Chemical Lagrangian Model of the Stratosphere (CLaMS) 2. Formulation of chemistry scheme and initialization, Journal of Geophysical Research, 107, https://doi.org/10.1029/2000JD000113, 2002b.

Molleker, S., Borrmann, S., Schlager, H., Luo, B., Frey, W., Klingebiel, M., Weigel, R., Ebert, M., Mitev, V., Matthey, R., Woiwode, W., Oelhaf, H., Dörnbrack, A., Stratmann, G., Grooß, J.-U., Günther, G., Vogel, B., Müller, R., Krämer, M., Meyer, J., and Cairo, F.: Microphysical properties of synoptic-scale polar stratospheric clouds: In situ measurements of unexpectedly large HNO₃-containing particles in the Arctic vortex, Atmospheric Chemistry and Physics, 14, 10 785–10 801, https://doi.org/10.5194/acp-14-10785-2014, 2014.

Nash, E. R., Newman, P. A., Rosenfield, J. E., and Schoeberl, M. R.: An objective determination of the polar vortex using Ertel's potential vorticity, Journal of Geophysical Research: Atmospheres, 101, 9471–9478, https://doi.org/10.1029/96JD00066, 1996.

Northway, M. J., Gao, R. S., Popp, P. J., Holecek, J. C., Fahey, D. W., Carslaw, K. S., Tolbert, M. A., Lait, L. R., Dhaniyala, S., Flagan, R. C., Wennberg, P. O., Mahoney, M. J., Herman, R. L., Toon, G. C., and Bui, T. P.: An analysis of large HNO_3-containing particles sampled in the Arctic stratosphere during the winter of 1999/2000, Journal of Geophysical Research: Atmospheres, 107, SOL 41–1–SOL 41–22, https://doi.org/10.1029/2001JD001079, https://agupubs.onlinelibrary.wiley.com/doi/abs/10.1029/2001JD001079, 2002.

Pitts, M. C., Poole, L. R., and Gonzalez, R.: Polar stratospheric cloud climatology based on CALIPSO spaceborne lidar measurements from 2006 to 2017, Atmospheric Chemistry and Physics, 18, 10 881–10 913, https://doi.org/10.5194/acp-18-10881-2018, https://www.atmos-chem-phys.net/18/10881/2018/, 2018.

Popp, P. J., Northway, M. J., Holecek, J. C., Gao, R. S., Fahey, D. W., Elkins, J. W., Hurst, D. F., Romashkin, P. A., Toon, G. C., Sen, B., Schauffler, S. M., Salawitch, R. J., Webster, C. R., Herman, R. L., Jost, H., Bui, T. P., Newman, P. A., and Lait, L. R.: Severe and extensive denitrification in the 1999-2000 Arctic winter stratosphere, Geophysical Research Letters, 28, 2875–2878, https://doi.org/10.1029/2001GL013132, 2001.

Rex, M., Salawitch, R. J., Deckelmann, H., von der Gathen, P., Harris, N. R. P., Chipperfield, M. P., Naujokat, B., Reimer, E., Allaart, M., Andersen, S. B., Bevilacqua, R., Braathen, G. O., Claude, H., Davies, J., de Backer, H., Dier, H., Dorokhov, V., Fast, H., Gerding, M., Godin-Beekmann, S., Hoppel, K., Johnson, B., Kyrö, E., Litynska, Z., Moore, D., Nakane, H., Parrondo, M. C., Risley, A. D., Skrivankova, P., Stübi, R., Viatte, P., Yushkov, V., and Zerefos, C.: Arctic winter 2005: Implications for stratospheric ozone loss and climate change, Geophysical Research Letters, 33, 221, https://doi.org/10.1029/2006GL026731, 2006.

Riese, M., Ploeger, F., Rap, A., Vogel, B., Konopka, P., Dameris, M., and Forster, P.: Impact of uncertainties in atmospheric mixing on simulated UTLS composition and related radiative effects, Journal of Geophysical Research: Atmospheres, 117, n/a–n/a, https://doi.org/10.1029/2012JD017751, 2012.

Riese, M., Oelhaf, H., Preusse, P., Blank, J., Ern, M., Friedl-Vallon, F., Fischer, H., Guggenmoser, T., Höpfner, M., Hoor, P., Kaufmann, M., Orphal, J., Plöger, F., Spang, R., Suminska-Ebersoldt, O., Ungermann, J., Vogel, B., and Woiwode, W.: Gimballed Limb Observer for Radiance Imaging of the Atmosphere (GLORIA) scientific objectives, Atmospheric Measurement Techniques, 7, 1915–1928, https://doi.org/10.5194/amt-7-1915-2014, 2014.

Santee, M. L., Manney, G. L., Froidevaux, L., Read, W. G., and Waters, J. W.: Six years of UARS Microwave Limb Sounder HNO3 observations: Seasonal, interhemispheric, and interannual variations in the lower stratosphere, Journal of Geophysical Research: Atmospheres, 104, 8225–8246, https://doi.org/10.1029/1998JD100089, https://agupubs.onlinelibrary.wiley.com/doi/abs/10.1029/1998JD100089, 1999.

Sinnhuber, B.-M., Stiller, G., Ruhnke, R., von Clarmann, T., Kellmann, S., and Aschmann, J.: Arctic winter 2010/2011 at the brink of an ozone hole, Geophysical Research Letters, 38, https://doi.org/10.1029/2011GL049784, 2011.

Stiller, G. P., von Clarmann, T., Funke, B., Glatthor, N., Hase, F., Höpfner, M., and Linden, A.: Sensitivity of trace gas abundances retrievals from infrared limb emission spectra to simplifying approximations in radiative transfer modelling, Journal of Quantitative Spectroscopy and Radiative Transfer, 72, 249 – 280, https://doi.org/https://doi.org/10.1016/S0022-4073(01)00123-6, http://www.sciencedirect.com/science/article/pii/S0022407301001236, 2002.

Stratmann, G., Ziereis, H., Stock, P., Brenninkmeijer, C., Zahn, A., Rauthe-Schöch, A., Velthoven, P., Schlager, H., and Volz-Thomas, A.: NO and NOy in the upper troposphere: Nine years of CARIBIC measurements onboard a passenger aircraft, Atmospheric Environment, 133, 93 – 111, https://doi.org/https://doi.org/10.1016/j.atmosenv.2016.02.035, http://www.sciencedirect.com/science/article/pii/S1352231016301480, 2016.

Tabazadeh, A. and Toon, O. B.: The presence of metastable HNO_3/H_2O solid phases in the stratosphere inferred from ER 2 data, Journal of Geophysical Research: Atmospheres, 101, 9071–9078, https://doi.org/10.1029/96JD00062, 1996.

Tritscher, I., Grooß, J.-U., Spang, R., Pitts, M. C., Poole, L. R., Müller, R., and Riese, M.: Lagrangian simulation of ice particles and resulting dehydration in the polar winter stratosphere, Atmospheric Chemistry and Physics Discussions, 2018, 1–32, https://doi.org/10.5194/acp-2018-337, https://www.atmos-chem-phys-discuss.net/acp-2018-337/, 2018.

Voigt, C., Dörnbrack, A., Wirth, M., Groß, S. M., Pitts, M. C., Poole, L. R., Baumann, R., Ehard, B., Sinnhuber, B.-M., Woiwode, W., and Oelhaf, H.: Widespread polar stratospheric ice clouds in the 2015–2016 Arctic winter – implications for ice nucleation, Atmospheric Chemistry and Physics, 18, 15 623–15 641, https://doi.org/10.5194/acp-18-15623-2018, https://www.atmos-chem-phys.net/18/15623/2018/, 2018.

Waibel, A. E.: Arctic Ozone Loss Due to Denitrification, Science (New York, N.Y.), 283, 2064–2069, https://doi.org/10.1126/science.283.5410.2064, 1999.

Waters, J. W., Froidevaux, L., Harwood, R. S., Jarnot, R. F., Pickett, H. M., Read, W. G., Siegel, P. H., Cofield, R. E., Filipiak, M. J., Flower, D. A., Holden, J. R., Lau, G. K., Livesey, N. J., Manney, G. L., Pumphrey, H. C., Santee, M. L., Wu, D. L., Cuddy, D. T., Lay, R. R., Loo, M. S., Perun, V. S., Schwartz, M. J., Stek, P. C., Thurstans, R. P., Boyles, M. A., Chandra, K. M., Chavez, M. C., Chen, G.-S., Chudasama, B. V., Dodge, R., Fuller, R. A., Girard, M. A., Jiang, J. H., Jiang, Y., Knosp, B. W., LaBelle, R. C., Lam, J. C., Lee, K. A., Miller, D., Oswald, J. E., Patel, N. C., Pukala, D. M., Quintero, O., Scaff, D. M., van Snyder, W., Tope, M. C., Wagner, P. A., and Walch, M. J.:

The Earth observing system microwave limb sounder (EOS MLS) on the aura Satellite, IEEE Transactions on Geoscience and Remote Sensing, 44, 1075–1092, https://doi.org/10.1109/TGRS.2006.873771, 2006.

Werner, A., Volk, C. M., Ivanova, E. V., Wetter, T., Schiller, C., Schlager, H., and Konopka, P.: Quantifying transport into the Arctic lowermost stratosphere, Atmospheric Chemistry and Physics, 10, 11 623–11 639, https://doi.org/10.5194/acp-10-11623-2010, https://www.atmos-chem-phys.net/10/11623/2010/, 2010.

Woiwode, W., Grooß, J.-U., Oelhaf, H., Molleker, S., Borrmann, S., Ebersoldt, A., Frey, W., Gulde, T., Khaykin, S., Maucher, G., Piesch, C., and Orphal, J.: Denitrification by large NAT particles: The impact of reduced settling velocities and hints on particle characteristics, Atmospheric Chemistry and Physics, 14, 11 525–11 544, https://doi.org/10.5194/acp-14-11525-2014, 2014.

Woiwode, W., Höpfner, M., Bi, L., Pitts, M. C., Poole, L. R., Oelhaf, H., Molleker, S., Borrmann, S., Klingebiel, M., Belyaev, G., Ebersoldt, A., Griessbach, S., Grooß, J.-U., Gulde, T., Krämer, M., Maucher, G., Piesch, C., Rolf, C., Sartorius, C., Spang, R., and Orphal, J.: Spectroscopic evidence of large aspherical β-NAT particles involved in denitrification in the December 2011 Arctic stratosphere, Atmospheric Chemistry and Physics, 16, 9505–9532, https://doi.org/10.5194/acp-16-9505-2016, 2016.

Zhu, Y., Toon, O. B., Pitts, M. C., Lambert, A., Bardeen, C., and Kinnison, D. E.: Comparing simulated PSC optical properties with CALIPSO observations during the 2010 Antarctic winter, Journal of Geophysical Research: Atmospheres, 122, 1175–1202, https://doi.org/10.1002/2016JD025191, https://agupubs.onlinelibrary.wiley.com/doi/abs/10.1002/2016JD025191, 2017.

Ziereis, H., Minikin, A., Schlager, H., Gayet, J. F., Auriol, F., Stock, P., Baehr, J., Petzold, A., Schumann, U., Weinheimer, A., Ridley, B., and Ström, J.: Uptake of reactive nitrogen on cirrus cloud particles during INCA, Geophysical Research Letters, 31, https://doi.org/10.1029/2003GL018794, https://agupubs.onlinelibrary.wiley.com/doi/abs/10.1029/2003GL018794, 2004.